Rotational spectrum of the 2-fluoroethanol---water complex: water tunneling dynamics and structure

by

Wenyuan Huang

A thesis submitted in partial fulfillment of the requirements for the degree of

Master of Science

Department of Chemistry
University of Alberta

Abstract

The hydrogen-bonded complexes between 2-fluoroethanol and water molecules have been investigated by using Fourier transform microwave spectroscopy and ab initio calculations. The computational and experimental theories are briefly described. The instrumentation and theoretical consideration about two primary spectrometers I used during the thesis studies, namely the cavity-based and the chirped-pulse Fourier transform microwave spectrometers, are discussed. The fluorinated ethanol and water cosolvent has been long studied due to its capability to alter the secondary and tertiary structures of the proteins and polypeptides. The mechanism is still mysterious but hydrogen bonds are believed to play an important role during this process. Thus it is worthwhile to develop a comprehensive molecular level understanding of the associated hydrogen-bonded complexes. The hydrogen-bonded topologies of the 2-fluoroethanol···water binary adduct have been probed from the rotational spectra in the frequency range of using the jet pulsed Fourier transform microwave spectrometers in combination with high level ab initio calculations. The assignments for the most stable 2-fluoroethanol···water complex along with its deuterium substituted isotopolugues have been achieved. The analyses of the spectroscopic date reveal the strong preference of the insertion geometry. Each rotational transition in the parent isotopologue is split into a doublet due to the tunneling motion of interchange in the hydrogen-bonded and non-bonded hydrogens of water. The tunneling assignment has been further proved by the intensity ratios as well as the isotopolugues. The tunneling has also been investigated through the transition state calculation and potential energy scan. The 2-fluoroethanol···$(water)_2$ complexes have also been optimized and several true minima have been identified. The result of my studies confirms the insertion binding topology is favorable in the formation of monohydrate of 2-fluoroethanol. The same preference was reported for the 2,2,2-trifluoroethaonl···water.

Preface

This thesis is based on the research I have done at the University of Alberta between September 2014 and January 2017. Chapter 3 of this thesis has been reproduced from a manuscript under preparation: Huang, W.; Thomas, J.; Jäger, W.; Xu, Y. “Rotational spectroscopic study of the 2-fluoroethanol···water complex and its tunneling dynamics”. Dr. J. Thomas recorded the chirped pulsed spectrum and Prof. Y. Xu did the initial rotational spectroscopic assignment of the 2-fluoroethanol···water complex. I did the assignments of the seven isotopologues and all the analyses, as well as the related ab initio calculations. I wrote the first draft of the manuscript. Professor W. Jäger was involved with the experiments. Professor Y. Xu was the supervisor author and was involved in the concept formation, as well as manuscript composition.

Dedicated to my loving parents

Acknowledgement

I would like to express my deepest gratitude to my supervisor Prof. Yunjie Xu for her guidance, encouragement and gracious support throughout my thesis research, for her expertise in the field that directed this research and for her support and faith in me at every stage. It would never have been possible to finish this thesis research without her selfless assistance. Keen scientific interest and attention to detail are two of the characteristics that I am most thankful to learn from Yunjie.

I would like to thank Prof. Wolfgang Jäger for providing the instruments and many insights. He is a really brilliant scientist who can always bring up ideas that others overlooked. I am also thankful to Prof. Michael Serpe and Prof. John Klassen, my supervisory committee members, for their generous suggestions. I wish to express my sincere gratitude to my external examiner Prof. Alex Brown, who provided numerous suggestions and revisions for my thesis presentation and paper. Thanks to Prof. Gabriel Hanna for readily agreeing to be my examiner. Special thanks to Dr. Norman Gee for being my teaching assistant coordinator.

I am particularly thankful to Javix Thomas, my mentor, long time office-mate, and true friend. I would not have been able to accomplish many research tasks or get on track without him. Beyond the postdoctoral fellow-graduate student mentorship, we also enjoy time sharing experiences and inspirations. Wherever he is, I wish him all the best of luck in his endeavors.

Also, I am grateful to learn from and share discussions with many knowledgeable and friendly group members. I express my special thanks to Elijah, Matthias, and Nate for their helpful suggestions and discussions about theoretical calculations. I would also like to thank Jiao, Amin, Angelo, Joseph, Leo, Prasanta, Supriya, Chrissy, Jasmine, Fan, Jerry, Dan, Xiaoli, Anna and Alberto for their friendship and support.

I am grateful to all my friends for being there for me through years. I owe the biggest thanks to my parents for their unconditional support and endless love.

Table of Contents

List of Tables

List of Figures

List of Symbols

ρ	Electron density
$\hat{H}$	Hamiltonian operator
Ψ	Time independent wave function
K	Boltzmann constant
$\varphi_{rot,i}$	Initial state rotational wave function
$\varphi^*_{rot,f}$	Final state rotational wave function
$\hat{\mu}_g$	Dipole moment operator
J	Rotational level
$E_{rot}(J)$	Rotational energy
$\hat{I}$	Moment of inertia
$\Psi_J^M(\theta, \phi)$	Spherical harmonics
$P_J^{\|M\|}$	Associated Legendre polynomial
A, B, C	Rotational constants
μ_a, μ_b, μ_c	Dipole moment components
J_{KaKc}	Rotational level
T_2	Macroscopic polarization decays rate
ω_R	Rabi frequency
μ_{12}	Electric dipole moment of the transition between level 1 and 2
Q	Quality factor of the cavity

List of Abbreviations

HF	Hartree Fock method
MP2	Møller Plesset perturbation theory of second order
DFT	Density functional theory
BSSE	Basis set superposition error
CP	Counterpoise correction scheme
FTMW	Fourier Transform microwave spectrometer
AWG	arbitrary waveform generator
TTL	transistor-transistor logic
RF	radio frequency
CP-FTMW	Chirped pulse Fourier transform microwave spectrometer
2-FE	2-fluoroethanol
IR	Infrared
B3LYP	Becke, three-parameter, Lee-Yang-Parr
B3LYP-D3	Becke, three-parameter, Lee-Yang-Parr with D3 dispersion correction

Chapter 1

Introduction

1.1 Hydrogen bonding

Intermolecular interactions are the attraction and repulsion forces between neighboring molecules or groups of atoms. The presence of intermolecular interactions is going to affect several properties simultaneously, including physical ones like melting point, boiling point, solubility and viscosity, as well as chemical ones like thermodynamic stability, due to the structural change. The attractive interactions can be classified into ion-multipole, ion-induced multipole and Van der Waals interactions by the involved species. Van der Waals interactions can be further split into three contributions: Keesom interaction between permanent multipoles, Debye interaction between permanent and induced multipoles, and London dispersion force between induced multipoles.[1]

Hydrogen (H)-bonding, one special type of attractive interaction which is characterized by hydrogen atom bound to a region of high electron density,[2] has generated the earliest and everlasting research interest because of its importance in a wide range of fields. H-bonding influences the properties of water, an essential element of living, as well as a fundamental medium of chemical reactions. The double helical structure of DNA and the secondary and tertiary structure of proteins are also built based on H-bonding.[3] With such a significant and diverse role, fundamental study of the essence of H--bonding is of great importance.

H-bonding, is typically described as an electrostatic interaction between multipoles or induced multipoles.[2] However, unlike conventional Van der Waals interaction, H-bonding is directional and usually one-to-one corresponded. In some situations, one hydrogen atom can participate in two hydrogen bonds instead of one, forming the so-called 'bifurcated' hydrogen bonding. The bond energy of H-bonding varies from extremely weak (around 0.2-4 kcal/mol, which is in the same magnitude as London dispersion force) to as strong as about 40 kcal/mol, up to one third of a covalent bond. The bond length of a strong H-bond can be between 1.2 Å and 1.5 Å,[4] close to a covalent bond length. In a B-H···A type of hydrogen bond, the hydrogen-bonding can be intramolecular (both A and B atom belong to one molecule) or intermolecular (A and B atom belong to different molecules). Due to steric hindrance, the intramolecular H-bond often bends a bit and the B-H···A bond angle deviates from 180°, while for intermolecular H-bond the bond is less bent and has stronger preference to be straight. H-bonding not only can be found in solution, but also in the gas and in the solid phase.[5]

The earliest study of H-bonding cannot be attributed to a single scientist. Relevant concepts were raised in the early 20th century in German and English literature. Linus Pauling[6] credited T. S. Moore and T. F. Winmill in 1912 as the first to use the H-bonding concept to assign the trimethylammonium hydroxide structure in aqueous solution.[7] Further and more elaborated work from pioneer researchers like W. M. Latimer and W. H. Rodebush as well as M. L. Huggins[8] increased the interest in the H-bonding concept. In 1950-1960s, the traditional theory of H-bonding was established. Another surge of modern H-bonding studies begun in 1980s and continues to spark novel ideas.

Spectroscopic evidences have been commonly used to verify the existence of H-bonding interaction in the structural change and consequent properties variation. For example, the B-H stretch typically experiences a red shift in the related infrared and Raman spectra for H-bonding species, and normally is accompanied with the broadening of the band.[9] This shift can be ascribed to the formation of the H-bond which weakens the B-H bond. Related changes have also been identified in nuclear magnetic resonance spectroscopic studies since the proton involved in H-bonding experiences the deshielding effect, and is shifted to a lower field.[9] As the strength of the H-bond increases, leading to a shortening in the corresponding bond length, the proton is being further deshielded. Thus the H-bond length and the proton chemical shift exhibit a positive correlation which can be used to estimate the bond length. Some non-proton NMR studies can provide additional insight about the H-bonding interactions, for instance, O^{17} resonance of water and N^{15} resonance of ammonia.[3]

As H-bonding concept evolves, many unconventional hydrogen bonds with interesting characteristics began to draw more attention. The "unconventional" part of such bonds mainly addresses the extension of the range of H-bonding partners. Other electron-rich atoms or groups are taken into consideration. Compounds with π-bonds have been found to be good H-bond acceptors, either bonded to a polar hydrogen atom (H_p-π)[10, 11] or a nonpolar hydrogen atom (H-π or CH-π).[12, 13] The nonpolar hydrogen atom-π interaction mostly involves the hydrocarbyl hydrogen with a π acceptor and has a relatively small bond energy. In the polar hydrogen-π interactions, protons are attached to amino or hydroxyl groups, and are commonly expected to have a higher bonding energy.

Organometallic compounds have also been exploited extensively as they can be H-bonding acceptors or donors, and exhibit considerable potential in fundamental research of H-bond and practical applications in catalysis.[14] When serving as proton acceptors, organometallic compounds can mainly be divided into three groups: transition metal complexes, transition-metal hydride complexes and main-group metal hydride complexes. Sandwich complexes like Cp_2M and semi-sandwich complexes $CpML_n$, where Cp stands for cyclopentadienyl group and L= CO, NO etc., are classical proton acceptors for group VI-VIII transition metals. X-H···M bonds are formed in both intramolecular type and intermolecular type.[15] Organometallic hydrides can also act as proton donors, provided that the hydrides are in cationic form and have a relatively strong interaction with base ligand. $[Cp^*_2\text{-}OsH]^+$ and $[WH_5(dppe)_2]^+$ are found to be able to form hydrogen bond with PF_6^- and CF_3COO^-, confirmed by IR information.[16] The mechanism prior to proton transfer was proposed as $M^{\delta-}$ - $H^{\delta+}$ ··· B being the intermediate, in which the two species are linked by H-bonding. The Os-H stretching frequency at about 2160 cm^{-1} was red shifted after the mixing with strong N bases, as well as the red shift of B group spectra frequencies. Most of the organometallic H-bonds show medium strength and the bond energies are about 4-7.6 kcal/mol, and the linear arrangement of X-H···M still holds.

H-bonding affects many physical properties such as boiling point and melting points. For instance, from H_2S, H_2Se to H_2Te, the boiling point and melting point increase since the molar mass and dispersion force increase down the group VIA, but H_2O molecule has a much higher melting and boiling point than H_2S. This phenomenon is also found in group VA and VIIA for NH_3 and HF molecules, and can be ascribed to the existence of strong intermolecular H-bonds. Viscosity and density are properties that can as well show the influence of H-bonding in the molecule's physical appearance. With the formation of H-bond, molecule structure tends to stack in a more compact and oriented arrangement, thus raises the viscosity and density. Chemical properties like solvability and acidity are also closely related to H-bonding, and it's critical in electrolyte, ion cluster or acid-base chemistry to examine the strength of H-bond.

The secondary structure of protein is the transition from one-dimension to three-dimension, and such transformation requires the folding and bonding between different layers and chains. H-bonding, likely to happen between an amine group and another electronegative group, is the binder to hold the complex and site-specific three-dimensional structure of protein

in place. Similar functionality of H-bond is found in the case of cellulose, as the strong H-bonds ensures its crystal-like stability. In DNA/RNA, the H-bonding establishes a great number of intermolecular contacts such as a thymine-adenine pair where each has one H-bonding donor and acceptor site, and leads to the double helical structure. The H-bonding in proteins and DNAs not only stabilizes the bio macromolecules, but also brings flexibility and possibility of evolution, which are extremely important for the development of life.[17]

1.2 High resolution spectroscopic studies of H-bonding interactions

Although H-bonding exists in the gas, liquid and solid phases, it is difficult to study this interaction in condensed phase to gain detailed insight because of co-existence of many other interactions. One desirable way to study the H-bonding systems is by generating and stabilizing small H-bonded clusters in a supersonic jet expansion and interrogating them using various spectroscopic techniques. Many gas phase spectroscopic techniques have been applied for the studies of H-bonding, such as laser induced fluorescence,[18] resonance enhanced multiphoton ionization,[19] ultraviolet (UV)/ infrared (IR) double resonance,[20] Fourier transform IR spectroscopy[21] and IR multiphoton dissociation spectroscopy.[22] Most of the above studies have no rotational resolution and require the assistance of high level ab initio calculations to identify the carrier of a specific spectral feature observed. Moreover, some carriers with similar structures cannot be differentiated by the techniques mentioned above.

Rotational spectroscopy is directly sensitive to the mass distribution of a molecule and can provide the detailed information about H-bonding sites and topologies. Furthermore, with the Fourier transform microwave spectroscopic techniques used in this thesis studies (See Chapter 2), the experimental resolution for rotational spectroscopy is on the order of several kHz. This high resolution capability makes it possible to tell apart conformers with minor structural differences and also to resolve hyperfine structures such as tunneling components due to water tunneling motions. By optimizing the experimental pulse nozzle operating condition, one may

probe the stepwise solvation process by examining rotational spectra of hydrated clusters with increasing sizes.

So far, a great number of H-bonded systems have been investigated using rotational spectroscopy. These investigations include not only studies of the intramolecular H-bonded alcohols,[23] amines[24] and carboxylic acids,[25] but also the intermolecular H-bonded aggregates.[26] The intermolecular H-bonded systems can be formed between the same species, like the acrylic acid dimer[27] and the trifluoroethanol dimer,[28] or it can be formed between two different species, for example the ethanol-water[29] and the methyl lactate-ammonia[30] complexes. The studies of carboxylic acid dimers have probed the intriguing phenomena associated with proton tunneling effects between carboxylic groups.[31] H-bonded systems consisting of fluorinated compounds are also of significant interest due to the special properties associated with F element.[32] In the current thesis, I focus on rotational spectroscopy of the 2-fluoroethanol-water complex.

1.3 Outline of present study

The remainder of the thesis is divided into three sections. Chapter 2 includes discussion about both the experimental and theoretical details. In the theoretical portion, after a brief introduction of ab initio calculations, additional details associated with the current study, such as different levels of theory, methods and basis sets, are presented. The primary objective and interpretation of calculations are also discussed. The experimental section focuses on the two Fourier transform microwave spectroscopic instruments used, namely a cavity-based Fourier transform microwave spectrometer and a chirped-pulse Fourier microwave spectrometer, as well as the basic principle of rotational spectroscopy. A short summary of the several spectroscopic programs which I use to analyze the experimental data is also presented in this section.

Chapter 3 is the main part of my research. It is about the the 2-fluoroethanol-$(water)_{1,2}$ clusters, studied by using ab initio calculations and Fourier transform microwave spectroscopy. Details about the calculation results, experimental data and analyses in addition to the

interpretation of the outcome are shown in this chapter. The final conclusion and future work are described in chapter 4.

---

1. A. D. McNaught, A. Wilkinson, M. Nic, J. Jirat and B. Kosata, *IUPAC. Compendium of Chemical Terminology, 2nd ed. (the "Gold Book")*, Blackwell Scientific Publications, Oxford, 1997.
2. E. Arunan, G. R. Desiraju, R. A. Klein, J. Sadlej, S. Scheiner, I. Alkorta, D. C. Clary, R. H. Crabtree, J. J. Dannenberg and P. Hobza, *Pure and applied chemistry*, 2011, **83**, 1637-1641.
3. P. A. Kollman and L. C. Allen, *Chemical Reviews*, 1972, **72**, 283-303.
4. G. A. Jeffrey, *An Introduction to Hydrogen Bonding*, Oxford University Press, 1997.
5. T. Steiner, *Angewandte Chemie International Edition*, 2002, **41**, 48-76.
6. L. Pauling, *The Nature of the Chemical Bond and the Structure of Molecules and Crystals: An Introduction to Modern Structural Chemistry*, Cornell University Press, 1960.
7. T. S. Moore and T. F. Winmill, *Journal of the Chemical Society*, 1912, **101**, 1635-1676.
8. W. M. Latimer and W. H. Rodebush, *J. Am. Chem. Soc.*, 1920, **42**, 1419-1433.
9. A. S. N. Murthy and C. N. R. Rao, *Applied Spectroscopy Reviews*, 1968, **2**, 69-191.
10. K. Biradha and M. J. Zaworotko, *J. Am. Chem. Soc.*, 1998, **120**, 6431-6432.
11. L. S. Birchall, S. Roy, V. Jayawarna, M. Hughes, E. Irvine, G. T. Okorogheye, N. Saudi, E. De Santis, T. Tuttle and A. A. Edwards, *Chemical Science*, 2011, **2**, 1349-1355.
12. P. Ottiger, C. Pfaffen, R. Leist, S. Leutwyler, R. A. Bachorz and W. Klopper, *The Journal of Physical Chemistry B*, 2009, **113**, 2937-2943.
13. S. J. Grabowski and P. Lipkowski, *The Journal of Physical Chemistry A*, 2011, **115**, 4765-4773.
14. N. V. Belkova, E. S. Shubina and L. M. Epstein, *Accounts Chem Res*, 2005, **38**, 624-631.
15. E. S. Shubina, N. V. Belkova and L. M. Epstein, *Journal of Organometallic Chemistry*, 1997, **536**, 17-29.
16. L. M. Epstein, E. S. Shubina, A. N. Krylov, A. Z. Kreindlin and M. I. Rybinskaya, *Journal of Organometallic Chemistry*, 1993, **447**, 277-280.
17. Y. Marechal, *The Hydrogen Bond and the Water Molecule: The Physics and Chemistry of Water, Aqueous and Bio-Media*, Elsevier Science, 2006.
18. S. SenGupta, H. P. Upadhyaya, A. Kumar and P. D. Naik, *Chem Phys*, 2014, **443**, 8-16.
19. O. Dopfer, G. Lembach, T. G. Wright and K. Mullerdethlefs, *Journal of Chemical Physics*, 1993, **98**, 1933-1943.
20. M. Broquier, F. Lahmani, A. Zehnacker-Rentien, V. Brenner, P. Millie and A. Peremans, *Journal of Physical Chemistry A*, 2001, **105**, 6841-6850.
21. G. G. Yee, J. L. Fulton and R. D. Smith, *Journal of Physical Chemistry*, 1992, **96**, 6172-6181.
22. R. H. Wu and T. B. McMahon, *ChemPhysChem*, 2008, **9**, 2826-2835.

23. T. Goldstein, M. S. Snow and B. J. Howard, *Journal of Molecular Spectroscopy*, 2006, **236**, 1-10.
24. S. Melandri, A. Maris, P. G. Favero and W. Caminati, *ChemPhysChem*, 2001, **2**, 172-177.
25. S. Melandri, B. M. Giuliano, A. Maris, L. B. Favero, P. Ottaviani, B. Velino and W. Caminati, *Journal of Physical Chemistry A*, 2007, **111**, 9076-9079.
26. C. Perez, D. P. Zaleski, N. A. Seifert, B. Temelso, G. C. Shields, Z. Kisiel and B. H. Pate, *Angew. Chem.-Int. Edit.*, 2014, **53**, 14368-14372.
27. G. Feng, L. B. Favero, A. Maris, A. Vigorito, W. Caminati and R. Meyer, *J. Am. Chem. Soc.*, 2012, **134**, 19281-19286.
28. J. Thomas and Y. J. Xu, *Journal of Physical Chemistry Letters*, 2014, **5**, 1850-1855.
29. I. A. Finneran, P. B. Carroll, M. A. Allodi and G. A. Blake, *Physical Chemistry Chemical Physics*, 2015, **17**, 24210-24214.
30. C. Merten and Y. Xu, *Angewandte Chemie*, 2013, **52**, 2073-2076.
31. G. Feng, Q. Gou, L. Evangelisti and W. Caminati, *Angew. Chem.-Int. Edit.*, 2014, **53**, 530-534.
32. K. Brendel, H. Mäder, Y. Xu and W. Jäger, *Journal of Molecular Spectroscopy*, 2011, **268**, 47-52.

Chapter 2

Theoretical and experimental details

2.1 Ab initio calculation

Ab initio calculation methods are computational methods that are derived from quantum chemistry basics. The term 'ab initio' is a Latin term meaning 'from the beginning', and was first introduced in computational chemistry by D. P. Craig and I. G. Ross in a semi-empirical study on the excited states of the benzene molecule in 1950.[1] It is now accepted and used in the modern meaning 'from first principle of quantum mechanics',[2] and these accurate and well-defined calculation methods are widely used in solving physical and chemical problems.

The ab initio calculations rest on solving the Schrödinger equation, and different approximations can be used to simplify the procedure numerically. The approximations are not only helpful in improving efficiency and saving time, but are also necessary in obtaining the solutions. One important approximation is the Born-Oppenheimer approximation, which assumes the motion of atomic nuclei and electrons can be separated. The BO approximation enables the separation of electronic and nuclear wave functions, and it's mostly feasible because the mass of electrons are always negligible comparing to a nucleus.

Often there is a trade-off between accuracy and computational time when selecting ab initio calculation methods. Larger basis sets and fewer approximations generally provide more accurate calculation results. On the other hand, with large basis sets, the computational cost may increases drastically while the improvement is only marginal. Therefore an optimized or suitable method is encouraged to be used. Many ab initio methods have been developed such as Hartree-Fock (HF), restricted open-shell Hartree-Fock (ROHF), n-order Møller-Plesset perturbation theory (MPn), configuration interaction (CI) and coupled cluster (CC). HF method is one fundamental method in which the wave function ψ can be obtained after calculation of multiple numerical integrals. HF method intentionally ignores the explicit Coulombic electron-electron interaction and only use the average electronic field to simplify the calculation. As a result, HF method could not well describe the behavior of molecular systems in which the explicit Coulombic electron-electron interaction is important. Several post-HF methods, like CI, MPn and CC theory, build on the fundamental of HF calculations, and subsequently correct the electronic interactions. In CI calculations, the excitation of electrons to higher unoccupied molecular orbitals is introduced. A full-CI permits all possible electron excitations until all

electrons have been excited. Since it is computational demanding to include all excitations, CISD which truncates after the calculation of single and double excitations is a more realistic treatment. MP perturbation theory, also known as many-body perturbation theory, uses the perturbation theory to account for the electron correlation effects, usually to the second (MP2), third (MP3) or fourth (MP4) order. MP2 and MP4 theories are commonly applied in calculations of small molecular systems and show satisfying results when compared to the related experimental data. The advantages of the MP theory are time efficiency and size consistency.

In studies of H-bonding systems, the most widely used electron correlated method is the MP perturbation theory. MP2 theory has been proved to be extraordinary in capturing the key structural properties associated with H-bonding.[3] For the higher order MP theory (such as MP3 or MP4), despite the exponentially greater computation cost, the calculated results, however, does not outperform the MP2 theory in many cases in terms of agreement with the experiment. Thus, MP2 theory has been widely applied to probe conformational geometries and energies of H-bonding systems.[4, 5] I applied the same theory in this research.

Beside the ab initio methods, density functional methods, which use functionals to describe electron density, have also been used extensively and give reasonable results with low computational cost. One of the frequently used functional is the B3LYP method. It has been used extensively for H-bonding studies and shown to provide results with good agreement with experimental data.[5]

The ab initio methods convert the system into many integro-differential equations that must be solved numerically, and when it goes to larger molecular system, it's rather complicated to solve. The introduction of basis sets converts the difficulty of solving the Schrödinger equation, differential equations, into doing matrix multiplications and solving combination of linear equations, and thus greatly simplify the process by using linear algebra methods. There are many different types of basis sets composed of Gaussian-type orbitals, for instance, minimum basis sets and split-valance basis sets. It is critical to choose sufficiently large basis sets to obtain reliable outcome, taking computational costs into account as well, and the basis set applied in the present work is the Pople's spilt-valence basis sets such as 6-311G. Besides the extended basis sets, there are also several auxiliary functions which help to improve the performance of a basis set. In molecular environments, orbitals become distorted from their atomic shapes. Polarization

functions are introduced to account for the effects of polarization. This effect is usually more prominent for heavy atoms. Polarization functions are usually designated with "**" or (d, p), meaning that polarization functions are added to all atoms including H and He. In H-bonding system, inter- or intramolecular interactions happen at a distance longer than a regular chemical bond. It is important to properly describe electrons which are not tightly bound to the nuclei. We need functions that decay very slowly with the distance from nuclei and these functions are the diffuse functions designated with '++" in the Pople's notation. For example, in 6-311G++ (2d, p), '++' denote for one diffuse function for the s- and p-type Gaussian on heavy atoms and one diffuse function for the s-type Gaussian on H atoms.

There are three main objectives in carrying out computational study in my thesis research: 1) to identify all possible dominant conformers; 2) to have an estimate of the relative abundance of these conformers; 3) to predict the related spectroscopic properties such as rotational constants and electric dipole moment components. Some specific points have been considered in the energy calculation, as discussed below. Harmonic frequency calculations are used in conjunction with the geometry optimization calculations to identify any saddle points which have imaginary frequency and also to provide the zero-point energy. Both raw and zero-point energy corrected total energies are used to predict the relative stability of the H-bonded complexes in a jet expansion (vide infra). When applying the supramolecular method to compute the intermolecular interaction energy, one needs to take into account the basis set superposition errors (BSSEs). BSSEs arise because in the calculation of the complex, subunit_1 can 'utilize' the basis set of subunit_2 and vice versa, whereas in the related monomer calculations, this possibility of lower energy is not available in the monomer calculation. Even if we use the same basis sets for the two monomers and the corresponding complex, there is an inconsistency in the basis set size used for the complex versus for the monomers. One common procedure to account for the error is the counterpoise method by Boys and Bernardi,[6] in which the 'ghost atoms (orbitals)' are introduced in the monomer calculations.

2.2 Microwave spectroscopy and the related instruments

2.2.1 Introduction

Microwave spectroscopy coupled with supersonic jet expansion is one of the most powerful techniques to perform high resolution spectroscopic studies of a wide range of molecular systems from rare gas clusters, radicals and ions, to H-bonded clusters.[7] In my thesis, all rotational spectra have been recorded using a narrowband cavity-based Fourier-transform microwave spectrometer (FTMW) and a broadband chirped pulse FTMW spectrometer. Both spectrometers make use of a General Valve nozzle for supersonic jet expansion. Preliminary scans were first conducted on the broadband chirped-pulse FTMW spectrometer, and the final frequency measurements were carried out using the cavity-based FTMW spectrometer. I used several spectroscopic programs to do the spectral assignments and analyses. Details about the narrowband FTMW, broadband FTMW and the spectroscopic programs used are discussed in this section.

2.2.2 Microwave spectroscopy

Rotational transitions can be measured as absorption or emission of electromagnetic radiation typically in the microwave region (0.01 cm^{-1} – 100 cm^{-1} or 0.3 GHz – 3000 GHz). Pure rotational spectroscopy measures only the transitions between two different rotational states but in the same vibrational and electronic states, different from rotational-vibrational spectroscopy or ro-vibronic spectroscopy which also incorporate the changes in the vibrational and/or electronic states.

Since at room temperature, many rotational levels are populated, resulting in a huge number of possible rotational transitions and making it very difficult to achieve a rotational spectroscopic assignment. One solution to simplify the spectrum is to reduce the temperature. Once the molecule is cooled to a much lower temperature, the number of rotational levels populated is greatly reduced, resulting in a much simplified rotational spectrum. The regular cooling method is usually not suitable because as the sample is cooled, it will liquefy or solidify

before reaching the ideal low temperature. In the solid or liquid phase, molecules cannot rotate freely and one cannot observe their rotational spectra. One must find a way to decrease the temperature while maintaining a collision free environment. One possibility is to use a supersonic jet expansion.

Supersonic jet expansion was introduced by Kantrowitz and Gray in 1951 for the purpose of increasing molecular beams intensity.[8] In a supersonic jet expansion, a gas is expanded through a nozzle into a vacuum chamber. The diameter of the nozzle exit is specially selected so that it's much larger than the mean free path of the gas. The gas molecules will then collide with each other inside the nozzle orifice, and only those molecules that travel along the same direction along the nozzle exit will go through. The expansion provides a molecular ensemble which has almost the same velocity distribution in the same direction. For a monoatomic gas, because there is only translational energy, i.e., no vibrational or rotational energy, a supersonic jet expansion essentially leads to extremely cold translational temperature, i.e., almost the same translation speed for all. In the case of a polyatomic gas sample, we need to mix the sample gas with a noble gas. The collisions between the noble gas and sample molecules will cool down the sample molecules to a great extent. Before collision, the gas sample is at Boltzmann equilibrium with the same translation, rotational and vibrational temperature. Since rotational transition energy is generally much smaller than the difference between two vibrational states for polyatomic molecules, the subsequent collisions during a jet expansion typically can cool the translational and rotational temperatures most efficiently. After the expansion, the molecules are traveling in the same direction with similar velocity, creating a collision less environment. The translational, rotational, and vibrational temperatures are all different and the molecular ensemble is no longer at equilibrium. The typically translation temperature is a few mK and rotational temperature is about a few K. Thus, in the supersonic jet expansion environment, the cooling effect is not strongly relied on the physical properties of the molecule itself, but rather the design of the nozzle set up, the carrier gas used, and also the backing pressure. This advantage enables microwave spectroscopists to standardize the experimental procedures and simplifies the preparation of sample molecules.

A main requirement for rotational transitions to occur is that the molecule itself needs to have a permanent electric dipole moment so that it can interact with the electric-magnetic radiation. The line strength of a rotational transition is described by the following equation:

$$The\ probability\ of\ transition = \int \varphi_{rot,f}^{*} \hat{\mu}_g \varphi_{rot,i} d\tau$$

Where the $\varphi_{rot,f}^{*}$ is the complex conjugate of the final state wave function, $\varphi_{rot,i}$ is the initial state wave function and the $\hat{\mu}_g$ is the dipole moment operator in Cartesian coordinate. The integrand here must be an even function since the integration for an odd function from negative infinity to positive infinity is zero. Another criterion for making this integration meaningful is that the dipole moment component along the electric field axis must be non-zero, or as mentioned before, a permanent dipole moment is essential. The photon itself also constrains the transition because naturally one photon has only one unit of angular momentum, and it can only impart one unit of angular momentum to the molecule. Therefore, the transition for linear molecule has a selection rule that only the transition between rotational states with one rotational quantum number difference is allowed, or in other words,

$$\Delta J = \pm 1.$$

Whether a transition is allowed or not can be determined by the selection rule and the permanent dipole moment components. The intensity of an allowed transition is also related to the population difference between the final and initial rotational levels. The population distribution can be calculated by the Boltzmann distribution which expresses the population as a function of temperature.

$$\frac{n_J}{n_0} = \frac{e^{(-\frac{E_{rot}(J)}{RT})}}{\sum_{J=0}^{J=n} e^{(-\frac{E_{rot}(J)}{RT})}}$$

Where the $E_{rot}(J)$ is the energy of rotational state with quantum number equals to J, n_J is the population on single J rotational level and n_0 is the total number of molecules in the sample. Besides the distribution difference due to the rotational energies, the degeneracies of energy states also affect the total amount of molecules available on certain state. The degeneracy on rotational state J is 2J+1, and thus the overall population combining these two factors is

proportional to both (2J+1) and rotational energy. The population difference between final and initial states directly determines the strength of the transition, and the larger population difference will then have stronger transition intensity.

Generally, rotational spectra of molecules can be described using by a semi-rigid rotor model, i.e., with centrifugal distortion corrections. The rigid rotor model basically assumes that the molecule is rigid during rotation. The rotational eigenvalues can then be obtained by solving the related time independent Schrödinger equation:

$$\widehat{H}\Psi = \mathrm{E}\Psi$$

In order to solve the rotational energy levels for a rigid rotor, it is most convenient to use spherical polar coordinates. The Schrödinger equation in spherical coordinate takes the form for a diatomic or linear molecule:

$$\frac{\hbar}{2\hat{I}}\left[\frac{1}{\sin\theta}\frac{\partial}{\partial\theta}\left(\sin\theta\frac{\partial\Psi}{\partial\theta}\right)+\frac{1}{\sin^2\theta}\frac{\partial^2\Psi}{\partial\phi^2}\right]+E\Psi=0$$

Where the $\widehat{I}$ is the moment of inertia we could get from principal coordinate. Ψ is the rotational wavefunction and we use the separation of variables to solve this differential equation.

$$\Psi = \Theta(\theta)\Phi(\phi)$$

Here the θ and ϕ are different angular coordinates, and this product is called spherical harmonics. After separation of these two variables, the rotational wavefunction is a function of quantum number J and M.

$$\Psi_J^M(\theta,\phi) = N_{JM}P_J^{|M|}(cos\theta)e^{iM\phi}$$

Here N_{JM} is the normalization constant and $P_J^{|M|}(cos\theta)$ is the associated Legendre functions. The corresponding energy level for a linear rigid rotor is given by

$$E_J = \frac{\hbar}{2I}J(J+1) = BJ(J+1)$$

E_J is the energy for J rotational level with quantum number equals to J, which means the rotational energy levels are only related to the moments of inertia I and the J rotational quantum

numbers and it's irrelevant to M quantum number. It is also worthwhile to mention that the rotational level for quantum number J has a degeneracy equals to 2J+1, and this degeneracy is vanished at the presence of external electric field or magnetic field, which are known as Stark effect and Zeeman effect respectively.

For a rotating molecule, the distortion force will pull the molecule apart and increase the moments of inertia, thus decrease the B value. Therefore, to account for this deviation from rigid rotor case, centrifugal distortion correction term is added to modify the linear top rotational energy levels.

$$F(J) = BJ(J+1) - DJ^2(J+1)^2$$

Where D is the centrifugal distortion constant, and it is inverse proportional to the harmonic vibration frequency under the assumption of simple harmonic motion.

As discussed before, a rigid rotor model has a center of mass fixed in three-dimension space, and atoms rotate along its principal axes. The eigenvalues of this rotation motion are known as moments of inertia, denoted as I_A, I_B and I_C, depending on the corresponding principal axis (traditionally define as $I_A \leq I_B \leq I_C$). Based on different sets of moments of inertia, in microwave spectroscopy-the spectroscopy that essential measures rotational transitions-people normally divided molecules into several subgroups: linear tops ($I_A = 0, I_B = I_C$), spherical tops ($I_A = I_B = I_C$), symmetric tops including oblate symmetric tops($I_A = I_B < I_C$) and prolate tops($I_A < I_B = I_C$) and last but actually the most common situation, the asymmetric tops($I_A < I_B < I_C$). More details and representative molecules can be found in previous literature.[9]

The energy level for J rotational states of a linear top molecule is discussed above. For a symmetric top rotor, another rotational quantum number K needs to be introduced. In a symmetric top molecule, the energy of each rotational state is only determined by J and K quantum numbers.

$$E_{JK} = BJ(J+1) + (A-B)K^2 \text{ for prolate top}$$

$$E_{JK} = BJ(J+1) + (C-B)K^2 \text{ for oblate top}$$

Here the A, B and C are rotational constants which is related to the respective moments of inertia,

$$\mathrm{A} = \frac{h^2}{8\pi^2 I_A}$$

$$\mathrm{B} = \frac{h^2}{8\pi^2 I_B}$$

$$\mathrm{C} = \frac{h^2}{8\pi^2 I_C}$$

And the selection rules for symmetric top molecules are $\Delta \mathrm{J} = \pm 1, \Delta \mathrm{M} = 0, \pm 1, \Delta \mathrm{K} = 0$ and also the permanent dipole moment $\mu \neq 0$, which means transition can only happen between the same K-levels.

For asymmetric tops, the rotational Hamiltonian cannot be written in terms of the J operator, and the alternative way to solve the asymmetric case is by using the symmetric top basis sets and rewrite the wave function as a linear combination of that basis sets. Then through diagonalizing this representative matrix of Hamiltonian, one could obtain the energy levels for asymmetric tops by introducing two independent quantum numbers K_a and K_c. Now the total rotational level can be denoted as $J_{K_a K_c}$ where J is a good quantum number but K_a and K_c are not good quantum numbers but just representations of two extreme cases: prolate and oblate. The selection rules for asymmetric tops are similar to the symmetric tops, $\Delta \mathrm{J} = 0, \pm 1, \Delta \mathrm{M} = 0, \pm 1, \mathrm{J} \leq K_a + K_c \leq J + 1$. One important characteristic for asymmetric top rotors is that, since the three moments of inertia are all different from each other, the dipole moment components will affect the selection rules for K_a and K_c. Based on different dipole moment components along principal axis, the rotational transitions can be classified into three types:

For a-type transitions, in which case the $\mu_a \neq 0$, the $\Delta K_a = 0, \pm 2, \pm 4 \ldots and\ \Delta K_c = \pm 1, \pm 3, \pm 5 \ldots$;

For b-type transitions, in which case the $\mu_b \neq 0$, the $\Delta K_a = \pm 1, \pm 3, \pm 5 \ldots and\ \Delta K_c = \pm 1, \pm 3, \pm 5 \ldots$;

For c-type transitions, in which case the $\mu_c \neq 0$, the $\Delta K_a = \pm 1, \pm 3, \pm 5 \ldots and\ \Delta K_c = 0, \pm 2, \pm 4 \ldots$.

It is worthy to mention that generally the transitions with K_a or K_c value change larger than ± 1 are much weaker and are not commonly observed experimentally.

2.3 Microwave spectrometers

In this thesis study, two major microwave spectrometers are employed for the experimental studies. The narrow band cavity-based FTMW spectrometer has a narrow excitation bandwidth of several hundred kHz to 1 MHz, is usually used to measure a specific frequency with relatively high resolution. The chirped pulse FTMW spectrometer, instead, has a broader excitation bandwidth of 2 GHz and is used to scan a wide frequency range. Details about these two instruments are discussed in the following sections.

2.3.1 Narrow band cavity-based Fourier Transform Microwave Spectrometer

2.3.1.1 Introduction

At the beginning, different types of microwave spectrometers were applied to study the molecule structures, including the famous Stark's modulation experiment, in which a waveguide sample cell was used as the absorption cell.[10, 11] A commercial version of microwave spectrometers was developed by Hewlett Packard and widely used for fundamental research purpose. FTMW spectrometer was initially designed and constructed by Flygare and McGurk in 1975. Later on, Balle and Flygare demonstrated that by incorporating a Fabry-Perot cavity and a pulsed supersonic jet expansion, one could obtain much greater sensitivity. The Fabry-Perot cavity, which was used in Flygare and Balle's modified FTMW spectrometer, consisted of a pair

of spherical mirrors situating inside a vacuum chamber. The sample molecules were introduced as supersonic jet expansion beams through a pulse hole into the vacuum chamber and applied the microwave pulse afterwards. This Balle-Flygare FTMW spectrometer is one of the most commonly used microwave spectrometers nowadays due to its exceptionally high resolution and sensitivity and the capability of creating molecule clusters in a jet expansion. Here is a brief description about the principle and design of the Balle-Flygare FTMW spectrometer that is used in my thesis studies. Further details can also be found in the references.[12]

2.3.1.2 The Cavity-based FTMW Instrument

In a FTMW experiment, the sample is initially excited by a coherent microwave pulse, leading to the subsequent detection of the coherent spontaneous emission of the molecules as a function of time. The process is depicted in Figure 2.1.[13] The molecular dipoles inside the cavity are randomly oriented initially. The application of an intense coherent microwave pulse helps to align the molecules with permanent dipole moment (could be treated as electric dipoles). These dipoles then rotate in phase and with the same frequency with each other. The molecules now are in a superposition state of the upper and lower states, and they are oscillating with the transition frequency.

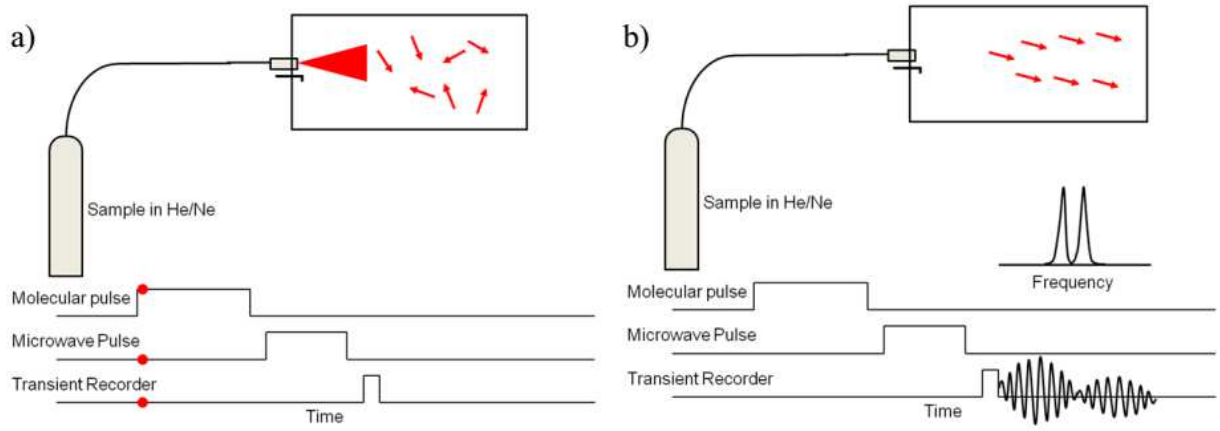

Figure 2. 1 Theoretical background of the FTMW spectroscopic technique. a) before and b) after the microwave excitation pulse

For a macroscopic polarization, the interaction of the molecules and electromagnetic field is well discussed in NMR or ESR (electro spin resonance) spectroscopy by calculating the Bloch equations.[14] After the interacting with microwave pulse, the wave functions of two rotational

states of the sample molecule will mix with each other and then a superposition state will be generated. Based on the Bloch equations, the way to generate macroscopic polarization, or in another word, to erase the population difference between two rotational states is applying a π/2 pulse of microwave spectroscopy. The definition of a π/2 pulse is that $\omega_R t = \frac{\pi}{2}$, where ω_R is Rabi frequency and t is the time period of microwave pulse. By applying this π/2 pulse, the molecules are equally populated on both rotational states, and the molecular ensembles are said to reach a macroscopic polarization, and the strength of the interaction is then optimized.

The criteria of a π/2 pulse indeed depends on the Rabi frequency, which is a measure of the interaction strength between the electric field of the microwave radiation and the electric dipole moment for a given transition. For a transition between state 1 and 2, the corresponding Rabi frequency is calculated by

$$\omega_R = \frac{\mu_{12}\epsilon}{\hbar} \; where \; \hbar = h/2\pi$$

Here the μ_{12} is the dipole moment and ϵ is the magnitude of the electric field of the microwave radiation. For molecules (or transitions) with a very small dipole moment (or components), a microwave power amplifier is introduced to amplify the excitation pulse.

The coherent excitation created a macroscopic polarization of the gas sample. This polarization is maximized by a π/2 pulse. After fine tuning, one could adjust the input microwave pulse so that the frequency is in resonant with certain rotational transition of the sample molecules. Owing to the fact that microwave pulse is normally much shorter than the macroscopic polarization decay time T_2, the signals after the decay of incident pulse is then dominated by the molecular emission signals. Upon the collection of this emitted signals as free induction decay in the time domain, Fourier transformation enables us to convert these time domain signals into frequency domain signals.

The cavity-based FTWM instrument I used in the thesis studies has been modified slightly from the original Balle-Flygare design.[15] The schematic diagram of the instrumental set up is provided in the diagram above (Figure 2.2). The red arrows show the detection part and the black arrows stand for the excitation part of the instrument.

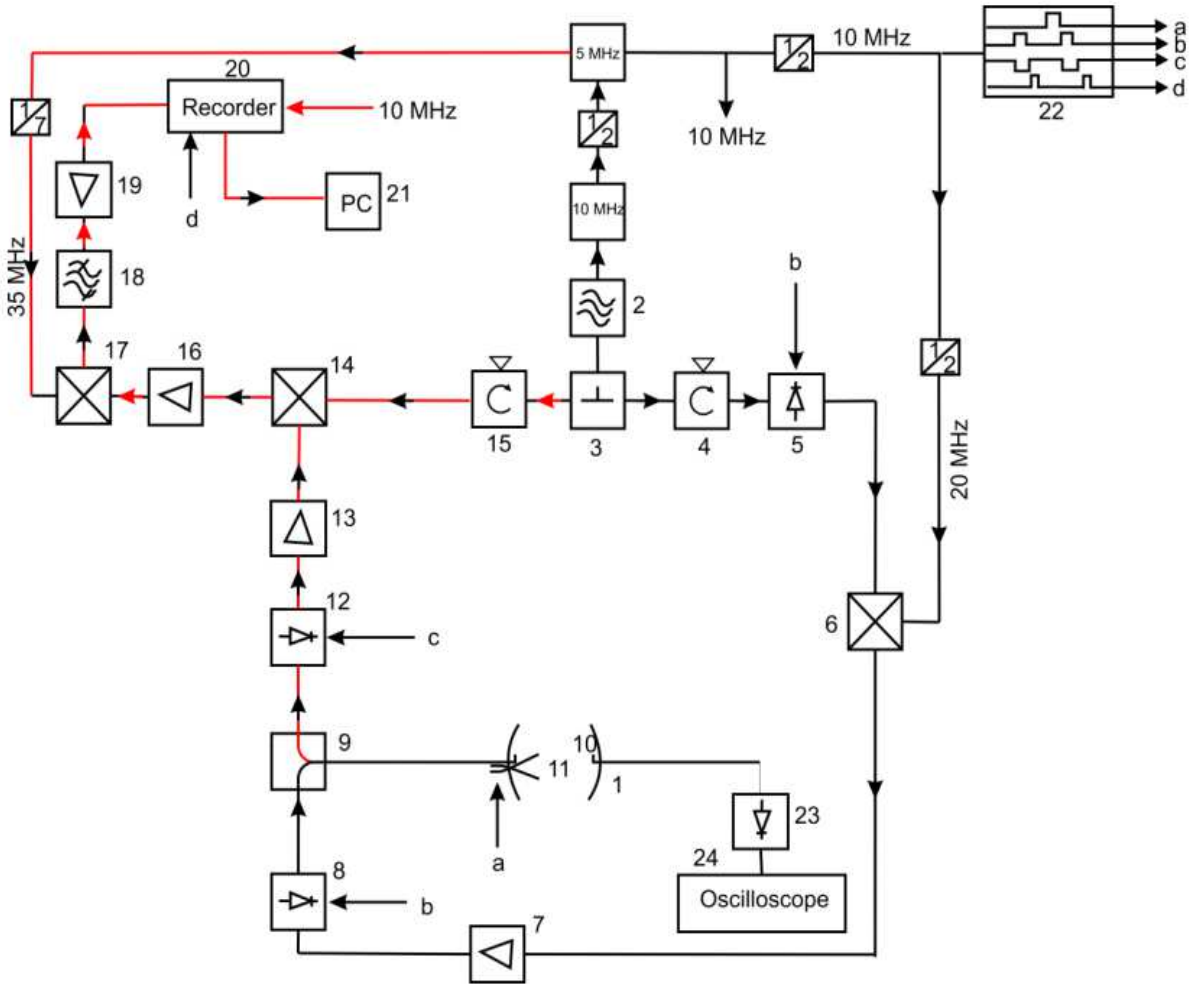

Figure 2. 2 A schematic diagram of the Balle-Flygare Fourier Transform Spectrometer (derived from Ref [15])

The components of the spectrometer are (1) nozzle, (2) Hewlett Packard MW synthesizer, (3) power divider, (4) isolator, (5) MW PIN switch, (6) 20 MHz double balanced mixer, (7) MW power amplifier, (8) MW PIN switch, (9) circulator, (10) antenna, (11) MW cavity, (12) MW PIN switch, (13) MW power amplifier, (14) image rejection mixer, (15) isolator, (16) radio frequency (RF) amplifier, (17) RF mixer, (18) 15 MHz band pass filter, (19) RF amplifier, (20) transient recorder, (21) personal computer, (22) pulse generator, and (23) detector.

1) Excitation arm

Not surprisingly, the excitation source of the FTMW spectrometer is a microwave synthesizer. The coherent microwave radiation that we used for the excitation is generated from the HP MW synthesizer (2). Then this microwave radiation is divided into two arms by the power divider (3): one arm goes to the cavity chamber and the other arm is for later mixing purpose. The excitation microwave pulse is then shaped by the MW PIN switch (5). A double balanced mixer (6) is used for the purpose of mixing the original microwave pulse with a 20 MHz signal and producing two sidebands that are 20 MHz away from the original frequency. The output signal from this mixer goes through a power amplifier (7) and another MW PIN switch (8) before the signal enters the cavity from the circulator (9).

2) Microwave cavity

The microwave excitation pulse, after passing the circulator, is introduced into the microwave cavity (11) through an L-shape antenna. The microwave cavity is the heart of this FTMW spectrometer, where the molecule ensemble interacts with the microwave pulse. This cavity is formed by two spherical aluminum mirrors and it can also serve as the sample cell. Each mirror has a diameter of 28 cm and the radius of curvature is 38 cm. One of the mirrors (actually it is the mirror that is close to the oscilloscope side) is fixed and the other mirror can be moved back and forth through a computer controlled motor. The distance between these mirrors are usually set to be between 20 and 40 cm. On the center of each mirror there is an L-shape antenna in order to collect the microwave radiation and molecular excitation. The antenna situated on the movable mirror collects the incident microwave radiation and then passes to the microwave detector (23) and shows on the oscilloscope (24). The whole cavity is placed in a vacuum chamber which is pumped by a 12-inch diffusion pump, and a roughing pump is applied to back the diffusion pump.

The purpose of adjusting the distance between mirrors using a motor is because one needs to tune the cavity into resonance. The standing wave patterns of a Farby-Perot cavity is one advantage of this cavity. The cavity could filter the microwave frequency since for a given separation between the mirrors, only under certain frequencies will be able to see the constructive interferences. All other frequencies will have destructive interferences and thus one needs to adjust the separation after tuning the incident microwave frequencies. Another huge advantage of Farby-Pero cavity is its high quality factor (Q). The quality factor is a measure of

energy storage ability of the resonator, defined as the ratio of energy stored in the resonator to the energy dissipation. The microwave experiment bandwidth is limited by both the quality factor and the bandwidth of original microwave pulse. In this cavity set up, the quality factor could be as high as 10,000, which means that the typical bandwidth is only about 1 MHz for a 10 GHz incident pulse. Since that the ordinary operating frequency range of this spectrometer is from 3-26 GHz, our experiments usually have a reasonably high resolution.

One tricky part of the cavity design is the coaxial propagation of the molecular beam. The nozzle (1), from which the supersonic jet expansion introduced the molecular beams into the cavity, is located at the center of the stationary mirror just below the antenna. The nozzle is orientated in the way that molecular beams is coaxial propagated relative to the cavity axis and the microwave pulse, therefore increases the interaction time between molecular and microwave pulse. The consequence of coaxial propagation is that it will reduce the spectral line width to several kHz and enables one to observe the hyperfine structure of very detailed splitting such as the proton transfer splitting in the 2-fluoroethanol···water complex. One other outcome of this orientation is that it will split all transitions into two Doppler components.

3) Detection arm

The output signal from the cavity can be represented as $\upsilon + 20MHz + \Delta\upsilon_m$, in which $\Delta\upsilon_m$ is the comparably weak molecular emission signal. This signal is detected by the antenna and coupled back to the detection arm of the microwave circuit through the same circulator (9). A third MW PIN switch is situated at the beginning of the detection arm for the sake of protecting the detection device from high power MW excitation pulse. The pulse then mixes with the original microwave pulse (υ) at the image rejection mixer (14) and becomes a down-converted signal with a frequency $20MHz + \Delta\upsilon_m$. Another radio frequency mixer (17) is used to further down-converted the signal the $15MHz + \Delta\upsilon_m$ and now this signal is eligible to be fed into the 15 MHz band pass filter (18). The final frequency signal in time domain is being recorded by the transient A/D recorder (20) and Fourier transformed into frequency domain spectra. The background subtraction is done for every experiment by collecting the background signal before addition of any sample and subtracting this from the final experimental signal.

4) Time sequence

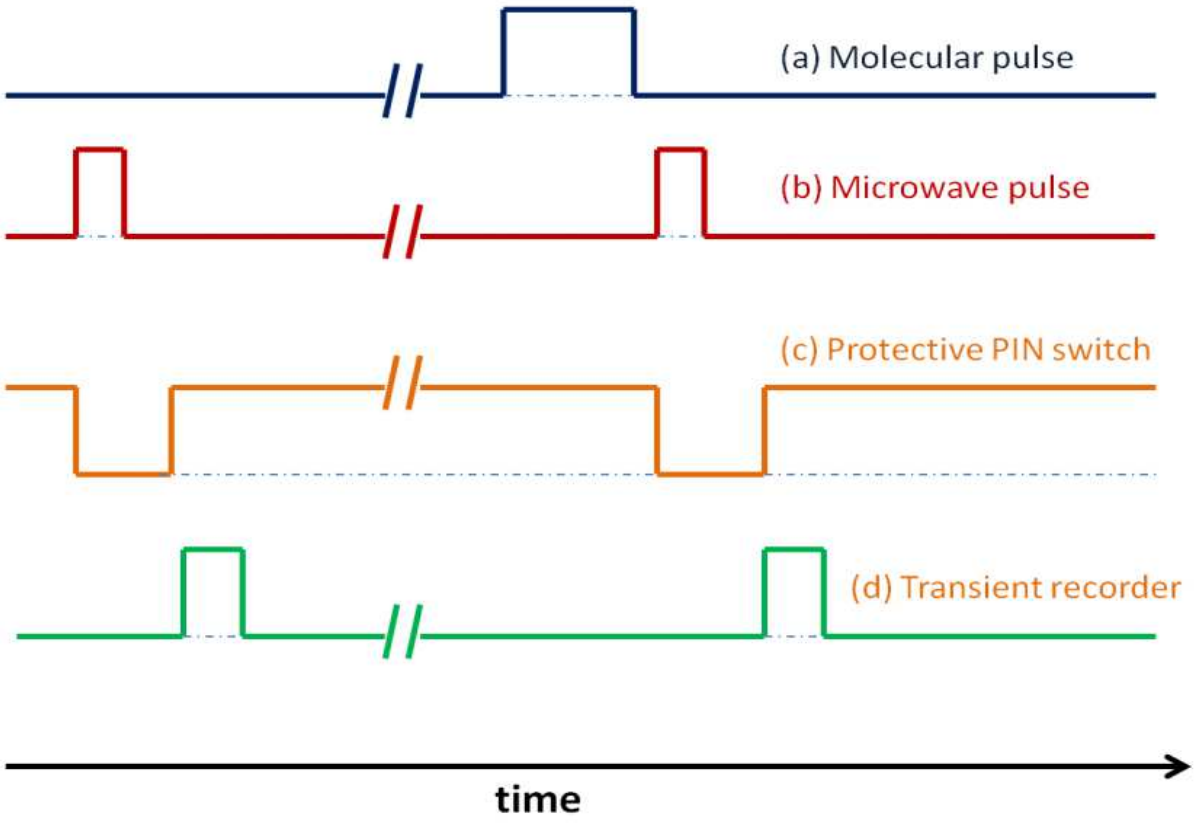

Figure 2. 3 A typical time sequence used in the cavity-based FTMW spectrometer

The proper timing of the events that happen in each cycling is critical for successful experiments, and the controlling train of transistor-transistor-logic or TTL pulses for cavity based FTMW spectrometer is depicted in Figure. Line (a) is the molecule pulse sequence, which means the opening window for nozzle to emit the molecular beam. It varies from 400-900 μs and it's adjustable. Line (b) stands for the microwave pulse sequence and it is generated around 10 μs after the end of molecular pulse. At the moment of opening the microwave pulse, the protective switch (12) also switches on for a longer period than that microwave pulse in order to protect the detection system from high power signal (as in line (c)). Eventually, as shown in line (d), about 10-25 μs after the end of microwave pulse, the comparably strong microwave signal decays sufficiently in the resonator and the data acquisition for molecular signal begins.

2.3.2 Broad band chirped-pulse Fourier Transform Microwave spectrometer

Since the introduction of Fabry-Perot cavity-based FTMW in 1981, this pulsed molecular beam spectrometer has become widely used thanks to its high resolution and sensitivity. Many further improvements have been made from the original spectrometer design, for the purposes of improving the sensitivity, expanding the measurement frequency range, optimizing the instrumental designs and introducing new pulsed value for unique gas phase molecular species. Those development continuously improved the performance of this microwave spectroscopy technique, but several fundamental operating problems were remained unsolved. One of the primary drawback of the cavity-based FTMW instrument is that the relative narrow excitation bandwidth, greatly limiting its application to molecular spectroscopic problems. The regular spectral bandwidth for our particular spectrometer is about 1 MHz, and if we want to do measurements for the next center frequency, one needs to tune the cavity into resonance for this specific frequency and the tuning takes much longer time than measurement itself. This makes the experiment over a large frequency region, e.g. 3 to 4 GHz for rotational spectra of the 2-fluoroethaonl···water complexes, very tedious and time inefficient. Although we have autoscan capability to automatically tune the cavity to resonance at every frequency step, it still takes more than 12 hours to scan a 100 MHz range. Another disadvantage of this cavity-based FTMW spectrometer, which is also a consequence of the narrow bandwidth, is that the relative line intensity across the spectra becomes less comparable. The line intensity hugely depends on the cavity modes, which is highly frequency sensitive, and therefore by simply adding the overlapping narrowband measurements may not be a good representation for the broadband spectra profile.

Thanks to the development of digital electronics, novel pulsed molecular beam FTMW spectrometer that enables the operation in broadband has been introduced by Pate's group at University of Virginia in 2008.[16] This new FTMW spectrometer, which is named chirped-pulse FTMW to emphasize the innovative microwave pulsed waveform used, could acquire the rotational spectrum over an 11 GHz frequency range for individual experimental cycle. The fast measuring speed, i.e. less than 10 μs for each date acquisition, a dramatic improvement compared to Fabry-Perot FTMW.

Several key components significantly affect the performance of this chirped pulse-FTMW. The arbitrary waveform generator (AWG) produces a chirped pulse waveform that creates a phase coherent, broadband linear frequency sweep. The high power amplifier boosts the incident microwave power for molecular excitation. And the ultrafast signal digitizer (40 Gsamples/sec) enables the high speed collection of rotational free induction decay signals and Fourier transformation subsequently. The experimental instrument I used for my thesis studies is the chirped pulse FTMW spectrometer developed in Dr. W. Jäger's group.[8, 17] The schematic diagram of this instrument is presented in Figure 2.4.

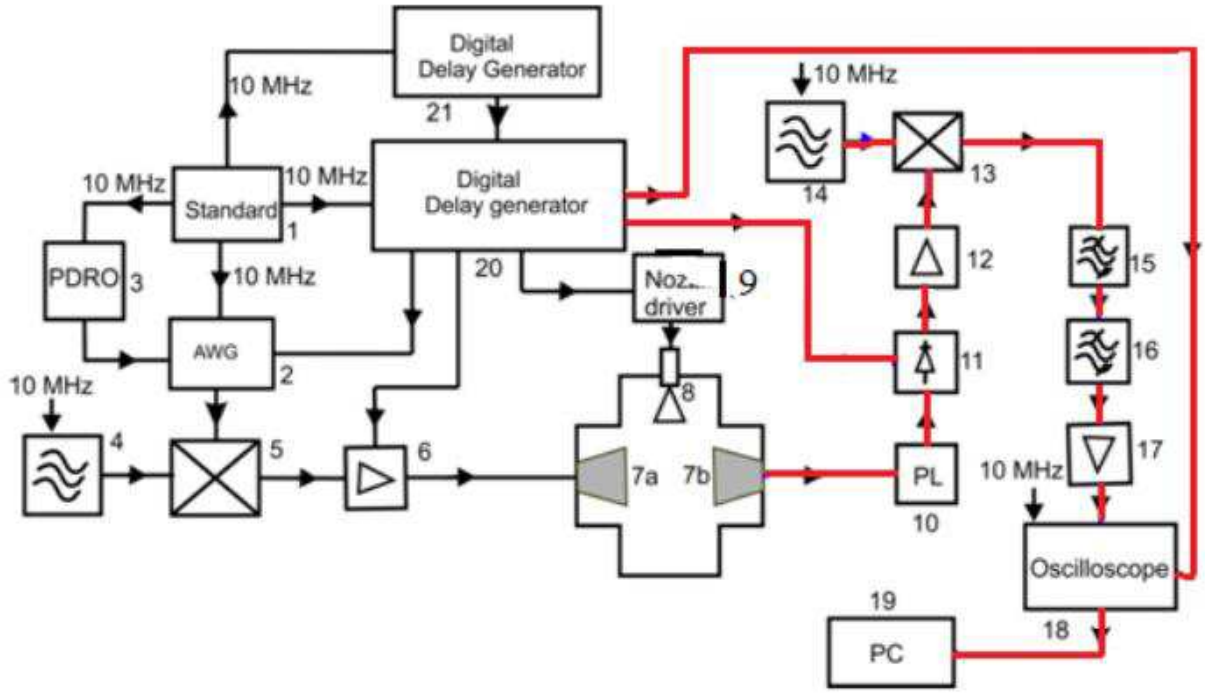

Figure 2. 4 A schematic diagram of the Chirped pulse Fourier Transform Spectrometer (derived from Ref [17]

The components shown in the above diagram are listed as follows: (1) Rb-frequency standard, (2) arbitrary waveform generator, (3) 3.96 GHz phase-locked dielectric resonator oscillator (PDRO), (4) synthesizer 1, (5) double balanced mixer, (6) 20 W solid state amplifier, (7) high gain horn antennas, (8) nozzle, (9) nozzle driver, (10) power limiter, (11) PIN diode switch, (12) low noise amplifier, (13) double balanced mixer, (14) synthesizer 2, (15) low pass filter, (16) low pass filter (17) low noise amplifier, (18) oscilloscope, (19) personal computer, (20) digital delay generator, and another (21) digital delay generator. The black arrows in the diagram represent the excitation arm, including the chirped-pulsed microwave source and the

molecular beam spectrometer, while the blue arrows stand for the detection arm that receives the molecular emission signals. The whole apparatus will be broken down into these three process and discussed in detail below.

1) Chirped-pulse microwave generation

The most critical component that symbolizes the CP-FTMW spectrometer must be the arbitrary waveform generator, which is programmed to produce the linear frequency sweeps of separately variable pulse duration and sweep range. This arbitrary waveform generator (AWG, item 2) is trigger by the 10 MHz reference signal from Rubidium-disciplined crystal oscillator (item 1) and referred to the external clock, the 3.96 GHz phase-locked dielectric resonator oscillator (PDRO, item 3). The PDRO also uses the 10 MHz Rb-oscillator reference frequency as its input so that the AWG and external clock are synchronized. The synchronization ensures the phase-stability of the AWG output signal over the full sweep frequency region and prevents the destructive interference between different phases. The chirped pulsed signal produced by AWG has a duration of 4 μs and sweep range from 0 to 1 GHz ($\Delta\nu$). This short duration is necessary in order to excite the molecules before the natural dephasing process of the rotational emission. The output pulse is then mixed with a fix MW frequency ν_{mw}, which is generated by the microwave synthesizer 1 (item 4) and synchronous with the reference signal, at the double balanced mixer (item 5). This mixing process produces a microwave pulse with a frequency centered at ν_{mw} and a bandwidth of 2 GHz, and one can tune the fixed frequency to shift the scanning region of interest. Unlike the cavity-based microwave spectrometer, the CP-FTMW chamber has no resonator to store the microwave power, so the input power for the excitation should be sufficiently high to efficiently polarize molecules in a large frequency range. In order to tune up the MW pulse power, a broadband 20 W high power solid state amplifier (item 6) is used to amplify the signal and the output of this amplifier is also under the control of same reference pulse to maintain phase stability. It has been estimated that for the excitation of molecules with a dipole moment of 0.7D over 11GHz range, the spectrometer requires 1kW amplifier to produce a 1 μs pulse. The amplified pulse is then broadcasted into the vacuum chamber through one horn antenna (item 7a) for the subsequent interaction with molecules.

2) Molecular beam spectrometer

Unlike the cavity chamber that has a pair of mirrors to adjust, the sample cell for CP-FTMW is relatively straight forward, consisting of a six-way cross aluminum chamber. The molecule of interest is introduced into the chamber as a supersonic jet expansion through a nozzle (item 8), which is driven by the nozzle drive (item 9). The chamber itself is vacuumed by a 1300L/s diffusion pump that is backed by a roughing pump, similar set up as cavity-based FTMW spectrometer for the sake of the maintenance of ultralow pressure. The microwave pulse is coupled into the vacuum chamber through one high gain horn antennas (item 7a) and propagates in a single direction through the chamber to the other identical horn antenna (item 7b). The second antenna is positioned approximately 30 cm from the entrance antenna and is used to collect the rotational free induction decay (FID) of the polarized molecules. Notice that the direction between the molecular beam pulse and microwave pulse is arranged perpendicular to each other, which is parallel in cavity-experiment to increase the interaction time. The perpendicular propagation set up, while reduces the time of interaction between pulses and detection of emission signal, prevents the Doppler splitting of the rotational transitions.

3) Emission signal detection

The output signals coming from the second antenna include the rotational FID as well as the original high power microwave polarization pulse. Therefore it is necessary to filter the high power microwave in order to obtain the much weaker emission signal. A pin diode power limiter (item 10) and a single pole single throw PIN diode switch (SPST, item 11) are placed before the low noise amplifier (item 12) and protect it from high power MW. The PIN diode switch is controlled to be closed during the polarizing pulse and open afterwards to pass the emission signal to the detection circuit. This filtered pulse then is amplified by the low noise amplifier before mixing with a second fixed MW pulse. The fixed MW pulse is generated by another synthesizer (item 14) and locked at a frequency that is 1.5 GHz higher than the original MW pulse (ν_{mw}+1.5). This 1.5 GHz is chosen to be higher than the upper limit of the frequency sweep, and therefore prevent the folding of the rotational spectrum. The microwave after mixing at the double balanced mixer (item 13), which ideally should have a frequency ranging from 0.5-2.5 GHz, is purified by two 4.4 GHz low pass filter (item 15, 16) to remove any high frequency artifact. After being amplified by a low noise amplifier (item 17), the emission signal finishes its processing and gets digitized with a fast digital oscilloscope (item 18). The digitization speed of

our oscilloscope is 40 Gs/s and its vertical resolution is 8-bits. The digitizer is also phase-locked to the reference Rb-oscillaor. A PC is used to fast Fourier transform the time-domain FID signal into frequency domain rotational spectrum. In order to achieve a well signal-to-noise ratio, normally 100 000 to 200 000 signals are averaged to obtain a high quality spectra. The frequency resolution of the CP-FTMW spectrometer is 25 kHz, and instrument is capable of doing 20 measurements during each microwave pulse. Each measurement includes one cycle of molecule polarization and signal detection. The background noise is measured before the molecule pulse in our experimental setup. An example of a broadband spectrum of the mixture between 2-fluoroethanol and water is presented below.

4) Time sequence

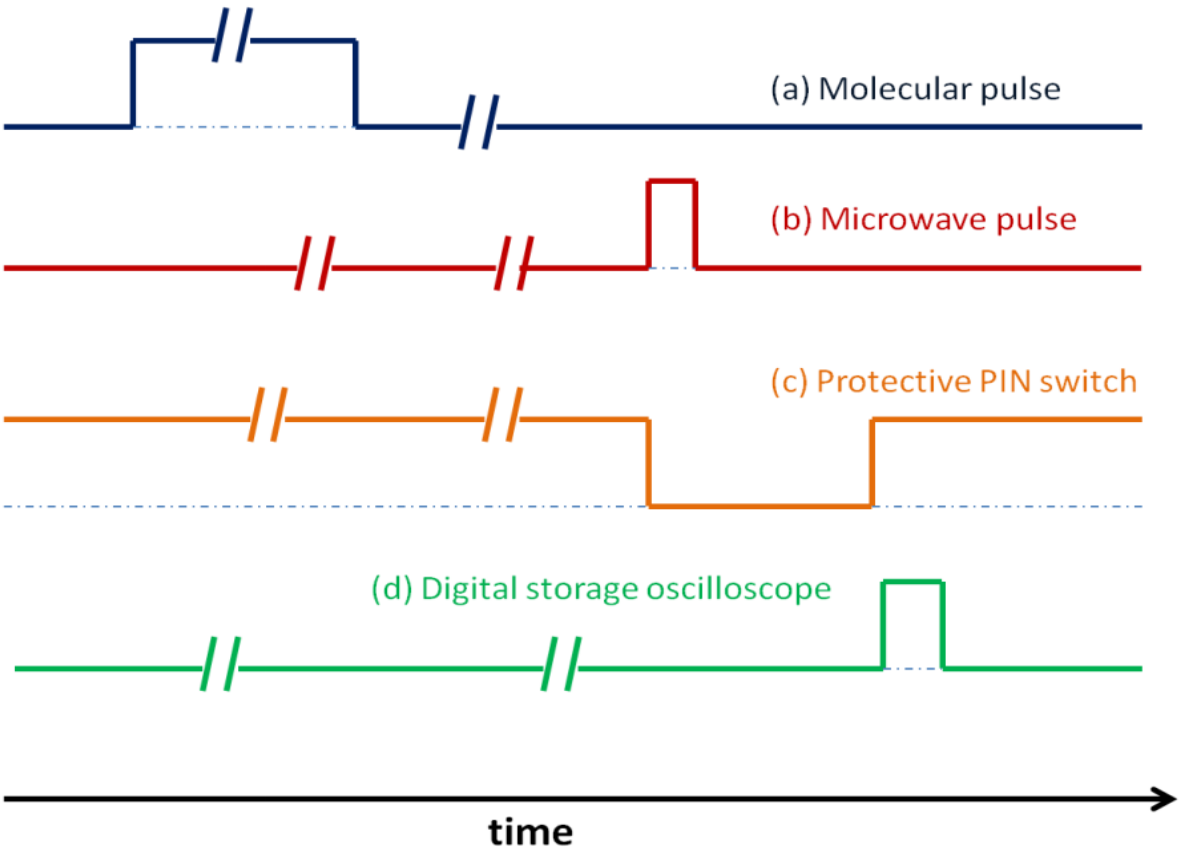

Figure 2. 5 A typical time sequence of the Chirped-pulse FTMW spectrometer.

A proper time sequence is crucial in order to acquire high quality chirped-pulse rotational spectra (Figure 2.5). For the sakes of phase stability between different points in time sequence, all the devices in the sequence must refer to the same reference Rb-frequency operation at 10

MHz. The TTL train of time within one cycle, which is shown in Figure, is controlled by the digital delay generator (item 20). The whole TTL signal controls the timing of the AWG, high power amplifier, nozzle driver, protective PIN switch and digital oscilloscope, according to the chronological order. One loop of these steps constitutes an experimental cycle, normally within several hundreds of microseconds. The timing between different cycles in controlled by another digital delay generator (item 21) to separate each cycles and prevent overlapping.

2.4 Some Spectroscopic Analysis Programs

Prediction of the rotational spectra are made using the rotational spectroscopic analysis programs developed, such as Pickett's program, Pgopher[18] and Autofit.[19] These programs are generously provided by the authors and available freely on their respective websites. I used mainly Pgopher because of its user-friendly graphical interface. Pgopher allows users to simulate the rotational spectra with several parameters like rotational constants, electric dipole moments and rotational temperature.

Broadband scans are typically done after obtaining a general idea about how the rotational spectrum of the targeted molecular system would look like using ab initio spectroscopic constants. The most informative regions are identified as the focus of the chirped scans. For H-bonded complexes, like my research system: 2-fluoroethano--water, one can obtain very dense broadband spectra. That is because these broadband spectra consist of the spectra of the monomers, the rare isotopologues of the monomers, the aggregates of these monomers, and of course the targeted complex, and larger mixed clusters with several 2-fluoroethanols and/or several water molecules. Therefore in order to aid the spectral assignment for a specific conformer, we often also record chirped spectrum with just 2-fluoroethanol or water so that one can remove lines not due to 2-fluoroethanol+water first. The remaining parts of the spectrum are then compared with the simulated spectra to look for a similar pattern of the molecules of desire. Once a rough assignment has been reached and the existence of the target molecular system has been confirmed, one can use the broadband spectra as a reference and go on to the cavity-based

FTMW for a high resolution measurement. With the reference spectra, no wide-range scan is needed on the cavity and this essentially eliminates its primary drawback. The measurement on cavity-based FTMW also allows one to detect possible hyperfine structures that are invisible in the broadband spectra.

Definite assignments are confirmed after the cavity measurements by using the Pgopher programs. Further theoretical calculation may be needed to interpret the difference, if any, between experimental results and initial prediction. For example, in my thesis study, there are significant discrepancy between the predicted and the observed geometry. One may need to examine potential energy surface in greater detail in order to interpret this difference. Further details are discussed in chapter 3.

---

1. R. G. Parr, D. P. Craig and I. G. Ross, *The Journal of chemical physics*, 1950, **18**, 1561-1563.
2. L. C. Allen and A. M. Karo, *Reviews of Modern Physics*, 1960, **32**, 275-285.
3. S. Scheiner, *Hydrogen Bonding: A Theoretical Perspective*, Oxford University Press, 1997.
4. G. Feng, Q. Gou, L. Evangelisti and W. Caminati, *Angew. Chem.-Int. Edit.*, 2014, **53**, 530-534.
5. J. Thomas, X. C. Liu, W. Jager and Y. J. Xu, *Angew. Chem.-Int. Edit.*, 2015, **54**, 11711-11715.
6. S. F. Boys and F. Bernardi, *Molecular Physics*, 1970, **19**, 553-566.
7. S. Melandri, D. Consalvo, W. Caminati and P. G. Favero, *Journal of Chemical Physics*, 1999, **111**, 3874-3879.
8. S. P. Dempster, O. Sukhorukov, Q.-Y. Lei and W. Jäger, *The Journal of chemical physics*, 2012, **137**, 174303.
9. F. X. Sunahori, N. Borho, X. Liu and Y. Xu, *The Journal of chemical physics*, 2011, **135**, 234310.
10. K. B. M. Jr., R. H. Hughes and E. B. W. Jr., *Review of Scientific Instruments*, 1949, **20**, 821-826.
11. R. H. Hughes and E. B. Wilson Jr, *Physical Review*, 1947, **71**, 562.
12. T. J. Balle, *Review of Scientific Instruments*, 1981, **52**, 33.
13. S. Ghosh and W. Jäger, master of science Thesis, University of Alberta, 2015.
14. S. Fölling, S. Trotzky, P. Cheinet, M. Feld, R. Saers, A. Widera, T. Müller and I. Bloch, *Nature*, 2007, **448**, 1029-1032.
15. Y. Xu and W. Jäger, *The Journal of chemical physics*, 1997, **106**, 7968-7980.

16. G. G. Brown, B. C. Dian, K. O. Douglass, S. M. Geyer, S. T. Shipman and B. H. Pate, *Review of Scientific Instruments*, 2008, **79**, 053103.
17. J. Thomas, J. Yiu, J. Rebling, W. Jager and Y. Xu, *The journal of physical chemistry. A*, 2013, **117**, 13249-13254.
18. C. M. Western, *University of Bristol: Bristol, U. K.* http://Pgopher.chm.bris.ac.uk.
19. N. A. Seifert, I. A. Finneran, C. Perez, D. P. Zaleski, J. L. Neill, A. L. Steber, R. D. Suenram, A. Lesarri, S. T. Shipman and B. H. Pate, *Journal of Molecular Spectroscopy*, 2015, **312**, 13-21.

Chapter 3

The Fourier transform microwave spectroscopy and ab initio calculations of 2-fluoroethanol and water complexes

3.1 Introduction

Fluoroethanols have been used extensively as a cosolvent for structural studies of proteins and polypeptides in aqueous solution. A small amount of fluoroethanol in aqueous solution can induce or destabilize the secondary or tertiary structures of proteins.[1] The mechanism behind this intervention of peptide binding by fluoroethanols has been investigated using nuclear magnetic resonance,[2] x-ray diffraction,[3] and circular dichroism[4] experimentally, and using molecular dynamic simulations theoretically.[5] Furthermore, due to the transient chirality of fluoroethanols, these solvents have become promising enantioselective catalysts in enantiomeric separation of chiral metal-organic frameworks, as demonstrated by solid-state NMR studies.[6] Despite a substantial body of research done to understand the above processes, a comprehensive understanding is still far away. The knowledge of the preferential binding sites and energetic preference among different conformers in the fluoroethanol-water complex is one essential step toward the final goal.

Intermolecular interactions between fluoroethanols, such as trifluoroethanol and 2-fluoroethanol (2-FE), with water and with ammonia have been the subjects of theoretical and experimental spectroscopic studies.[7-10] Low resolution supersonic jet Fourier transform infrared (FTIR) spectroscopy study reported by Heger et al.[11] monitored the OH stretching bands of mono-, di-, trifluoroethanol in their complexes with water and demonstrated that the water molecule acts as a hydrogen bond acceptor in all these cases. They attributed this to the high electron-withdrawing ability of the fluorine atoms within the fluoroethanol molecules, leading to decreasing electron density at the alcohol oxygen.

Supersonic jet expansion Fourier transform microwave spectroscopy (FTMW) has been used extensively in determination of structural and dynamical properties of small hydrogen-bonded molecular complexes including hydrated clusters.[12-15] This technique is highly sensitive to minor structural changes, such as –OH bond pointing direction, and offers a detailed picture about the geometry. In this study, we report the first high resolution rotational spectroscopy study of 2-FE···water complex, aided with ab initio calculations. We unambiguously assigned the most stable conformation of the complex and determined the non-bonded water OH pointing

direction using extensive isotopic studies. Furthermore, we compare the theoretical predictions with the experimental results and evaluate the quality of theoretical predictions.

3.2 Theoretical calculation

There are two critical dihedral angles in the 2-FE monomer: τ (FCCO) and τ (CCOH). Each of them can adopt three approximate values of 0°, +60° and -60°, corresponding to t/T, g+/G+, and g-/G- for τ (FCCO)/τ (CCOH), respectively. Base on the different combinations of these two angles, there are 9 possible monomer structures which include four mirror image pairs. They can be classified into five groups: G+g-/G-g+, G-t/G+t, Tt, Tg+/Tg- and G+g+/G-g-, in order of decreasing stability. Both theoretical and experimental results from previous studies[7] showed that the G+g-/G-g+ was the dominant conformer with about 7 kJ/mol stabilization energy. Some researchers attributed this to the intramolecular hydrogen bond between the hydroxyl hydrogen and the fluorine atom, although this aspect is still much debated.

Both insertion and addition topologies of intermolecular H-bond were considered when considering the 2-FE···H_2O complex. The relative raw dissociation energies (ΔD_e) of different geometries compared with the most stable conformer and the zero-point-energy (ZPE) corrected dissociation energies (ΔD_0) as well as the ZPE and BSSE corrected ones (ΔD_{e0}) are calculated. Spectroscopic constants for the three most stable conformers are summarized in Table 3.1 and their respective geometries are given in Figure 3.1. The insertion geometries are labeled beginning with letter i, while the addition geometries with a. The conformation of the 2-FE monomeric subunit is used next after the i/a labeling, followed by their rank based on the relative energies using Roman numbers. Based on the zero-energy corrected dissociation energy from calculation, it is fairly comfortable to say that iG+g- I and iG+g- II are the most possible geometries. It is worthy to notice that these two conformers are both insertion geometries based on the same G+g- monomer, when water is inserted into the existing F···HO contact, forming two new hydrogen bonds. The only difference between these two geometries is due to the flapping motion of the free hydrogen atom in water. Despite the fact that the rotational constants

of these two conformers are similar, their dipole moment components are much different. The c-type dipole moments, for example, is nearly zero for iG+g- I, while for iG+g- II, it's relatively large (2.31 Debye). This difference provides the possibility to differentiate these conformers based on their rotational spectra.

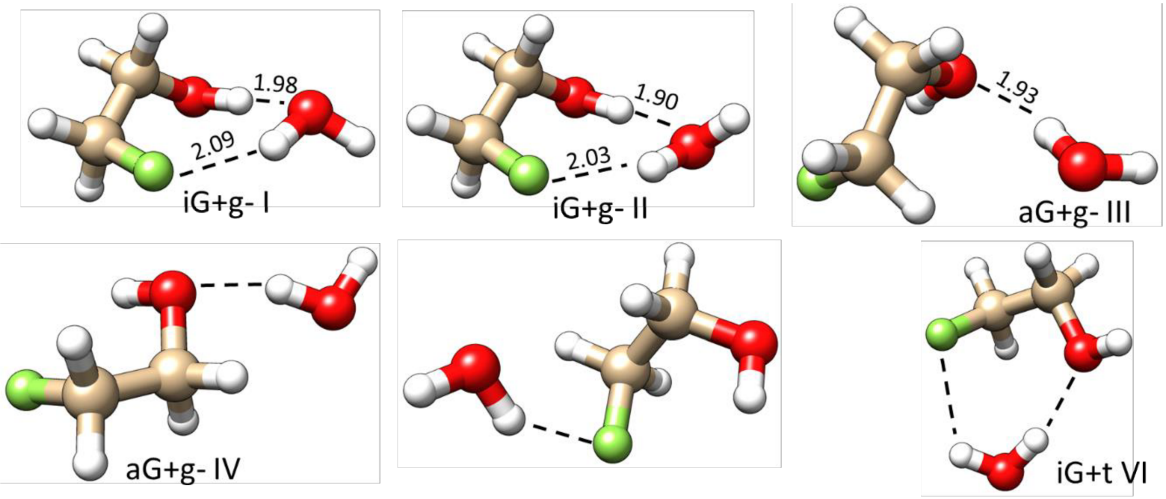

Figure 3. 1 Optimized geometries of 2-FE···water conformers at the MP2/6-311++ (2d,p) level. Intermolecular hydrogen bonds are indicated with dash lines.

Table 3. 1 ZPE corrected (ΔD_0) and ZPE&BSSE corrected ($\Delta D_{0,BSSE}$) energies (in kJ/mol), rotational constants (in MHz), and electric dipole moments (in Debye) of iG+g- I, iG+g- II and aG-g+ III, three most stable conformers of 2-fluoroethanol···water at the MP2/6-311++G(2d,p) level.

Parameters	iG+g- I	iG+g- II	aG-g+ III
ΔD_0[a] (kJ/mol)	0.00	0.79	3.78
$\Delta D_{0,BSSE}$[a] (kJ/mol)	0.00	0.70	2.14
A (MHz)	4945	4942	6307
B (MHz)	3447	3409	2395
C (MHz)	2216	2181	2092

$\lvert\mu_a\rvert$ (D)	0.38	0.77	0.20
$\lvert\mu_b\rvert$ (D)	1.61	1.58	0.87
$\lvert\mu_c\rvert$ (D)	0.12	2.31	0.60

[a] For the monohydrates, the ΔD_0 and $\Delta D_{0,BSSE}$ are relative to iG+g- I, the lowest energy conformer. $\Delta D_0(i)=D_0(iG+g- I)-D_0(i)$ and $\Delta D_{0,BSSE}(i)=D_{0,BSSE}(iG+g- I)-D_{0,BSSE}(i)$ where i=dimer I-III.

3.3 Experimental and computational details

The broadband chirped pulse FTMW spectrometer was used for the initial rotational spectra scan. The final measurements were done with the cavity-based FTMW spectrometer in the frequency range from 6 to 13 GHz. Both spectrometers are described in details in Chapter 2. The frequency uncertainty is ~ 2 kHz and the full width at half height is ~ 10 kHz for the cavity instrument and the corresponding values are ~ 5kHz and 25 kHz for the broadband spectrometer. Sample mixtures consisting of 0.13% of 2-FE and 0.10% of H_2O/D_2O in He/Ne at backing pressures of 2-5 bars were used for all measurements. 2-FE (99.99%, Sigma Aldrich), D_2O (98%, Aldrich), and Neon or Helium (99.9990%) were used without further purification.

All geometry optimization and harmonic frequency calculations, as well as the search of transition states were performed using the Gaussian09 program package[16] at the MP2/6-311++G (2d, p) level of theory. Optimized geometries were all confirmed to be at true minima without any imaginary frequencies. The calculated relative total energies for all the binary conformers identified were corrected for the zero-point-energy (ZPE) and also the basis set superposition errors (BSSEs) using the Boys and Bernardi's counterpoise method.[17]

3.4 Results and discussion

3.4.1 Rotational spectra and spectroscopic constants

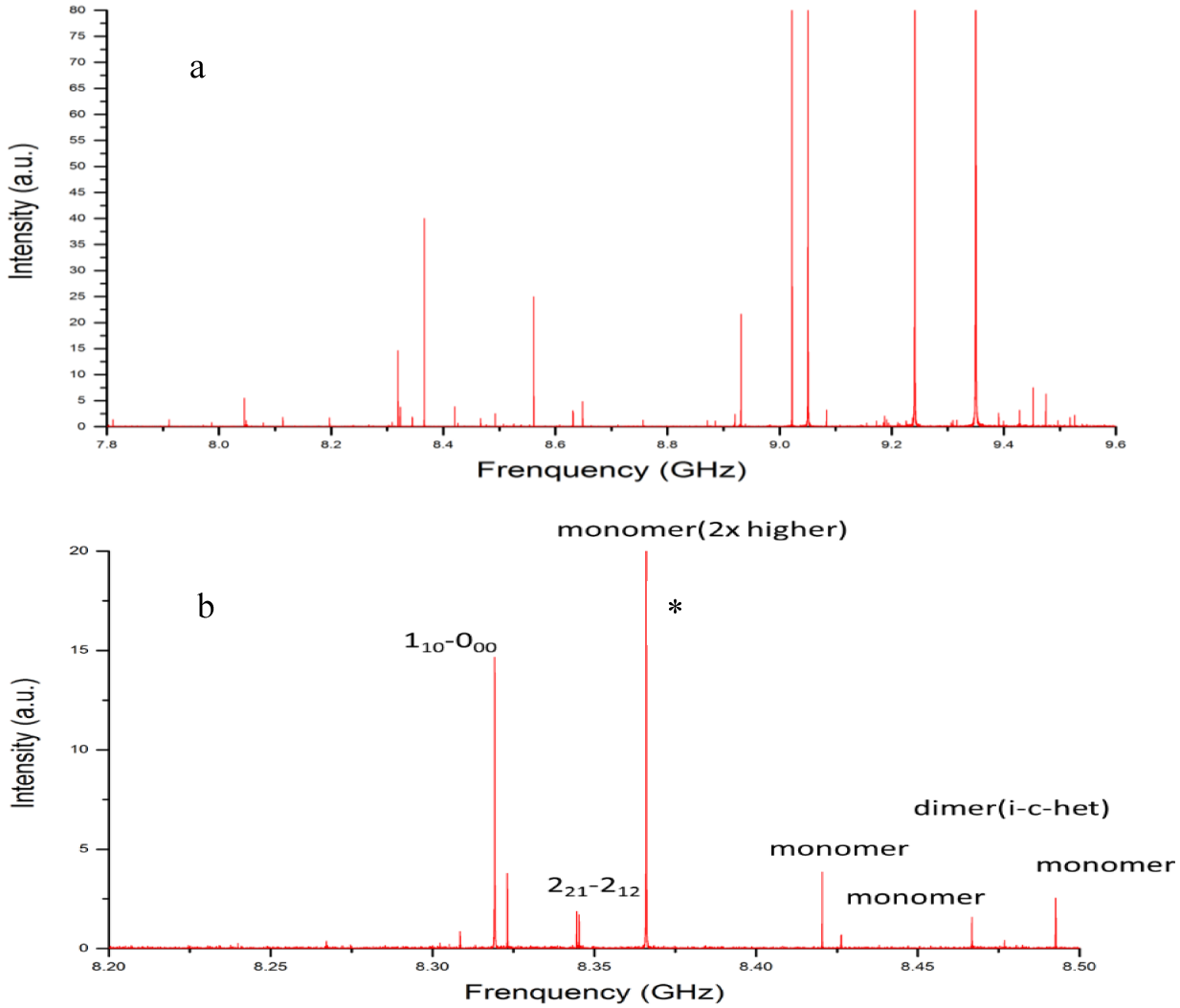

Figure 3. 2 a) A 0.8 GHz section of the broadband CP-FTMW spectrum of 2-FE and water complex system with 200,000 experimental cycles. b) An enlarged view of the 8.2 GHz-8.5GHz spectrum. The intensity of the monomer transition with * is twice as high as shown.

In the broadband rotational spectrum of produced by a mixture of 2-FE+H_2O+He contains transitions from many species (Figure 3.2). By comparing the spectra obtained with 2-FE+Ne, one can identify transitions including both 2-FE and water including the 2-FE···H_2O

complex. Both scans are recorded from 7.7 GHz to 11.3 GHz. One set of transitions were identified and assigned to the 2-FE···H_2O complex.

Final measurements with the cavity based FTMW spectrometer show that each rotational transition splits into two components with a relative intensity of roughly 3:1, with a splitting of several tens of kHz. This 3-to-1 ratio can be ascribed to the nuclear spin statistic weights for ortho (I=1) and para (I=0) hydrogen. Thus these tunneling splittings can be reasonably attributed to a tunneling motion which interchanges the bonded and non-bonded hydrogen atoms of water in the complex. The two components were fitted separately to Watson's S reduction semi-rigid rotor model using the Pgopher program.[18] The standard deviations of the fits are 2.7~2.8 kHz, which are approximately the experimental frequency uncertainty. Both sets of experimental spectroscopic constants are summarized in Table 3.2. The relative magnitudes of the electric dipole moment components were estimated base on the optimized microwave pulse widths for different type of transitions. All the observed transitions and the differences between the observed and calculated frequencies are for these two set tunneling motions are provided in Table 3.3. In particular, we noticed that the c-type transitions are also observed with fair intensity besides the a and b-types transitions. In fact that the experimentally estimated c-dipole component lies somewhere between that of iG+g- II and iG+g- I, although closer to II than I (vide infra).

Table 3. 2 Experimental spectroscopic constants for the 2-FE···H_2O conformers

Parameter	Para[a]	Ortho[a]
A (MHz)	4953.6265(15)[b]	4953.6551(14)
B (MHz)	3365.61604(91)	3365.6641(13)
C (MHz)	2171.79538(74)	2171.78790(85)
D_J (kHz)	3.766(43)	5.287(53)
D_{JK} (kHz)	1.63(42)	1.68(30)
D_K (kHz)	2.01(33)	2.22(24)
d_1 (kHz)	-1.267(21)	-2.387(27)

d_2 (kHz)	-0.646(17)	-0.537(20)
N[c]	22	21
σ (kHz)[d]	2.7	3.2

[a] Para and Ortho tunneling components due to the water tunneling motion. See text for details. [b] Errors in parentheses are in units of the last digit. [c] Number of lines fitted. [d] Standard deviation of the fit.

Table 3. 3 Measured rotational transition frequencies of the para and ortho states of the most stable monohydrate

J'	Ka'	Kc'	J"	Ka"	Kc"	Para		Ortho	
						ν_{exp}/kHz	Δν/kHz	ν_{exp}/MHz	Δν/kHz
1	1	1	0	0	0	7125.4017	-4.9	7125.4245	-1.3
2	0	2	1	1	0	7828.3701	-0.8	7828.3518	-0.6
1	1	0	0	0	0	8319.2198	2.7	8319.2809	-2.0
2	2	1	2	1	2	8345.4033	-0.4	8345.4679	3.0
2	2	0	2	1	2	8809.8846	1.3	8809.9701	0.7
2	0	2	1	1	1	9022.1854	4.0	9022.2066	-2.9
3	3	1	3	2	1	9183.3204	-0.4	9183.3345	2.7
2	1	2	1	1	1	9880.9145	-1.2	9880.9326	4.3
3	2	2	2	1	2			10386.8100	-4.3
2	0	2	1	0	1	10610.1973	5.6	10610.1973	-7.1
3	0	3	2	1	1	10644.3243	-3.2		
3	3	1	3	2	2	11175.0730	1.6	11175.1035	-3.6
4	1	3	4	0	4	11273.2887	0.1	11272.9882	-0.5
3	3	0	3	2	2	11298.7104	-1.5	11298.7544	1.5
2	1	2	1	0	1	11468.9262	0.3	11468.9262	3.0
2	1	1	1	1	0	12268.4737	-2.2	12268.5307	2.8
3	1	2	2	2	1	13263.9648	0.1	13263.9110	5.2
3	0	3	2	1	2	14225.6980	-0.2	14225.6875	-4.7
3	1	3	2	1	2	14570.4460	-3.9	14570.4460	-0.8
2	1	1	1	0	1	15050.2917	-5.0		
3	0	3	2	0	2	15084.4356	3.2	15084.4105	-0.5
3	1	3	2	0	2	15429.1877	3.5	15429.1657	0.1
2	2	1	1	1	0			17032.5391	3.1
2	2	0	1	1	0	17496.9895	1.0		

It is interesting to discuss further details about this binary adduct system. The result from rotational spectroscopy is consistent with the FTIR studies from Heger,[11] which demonstrated the strong preference of the insertion geometry over the addition binding topology. This preference is also in accordance with the theoretical dissociation energies, and can be attributed to the formation of stronger hydrogen bonds. The intramolecular H···F hydrogen bond originally in the 2-FE monomer (which has a theoretical bond length of 2.45Å) is replaced by two intermolecular hydrogen bonds between F···Hw (2.08 Å) and Ow···H (1.98 Å), which results in the stretching of H···F distance by 0.34 Å. Similar preference for the insertion binding geometry is observed for other small-molecule···H_2O or NH_3 binary adducts, for example in the TFE···water[9] and methyl lactate···H_2O[19] and methyl lactate···NH_3.[20]

3.4.2 Rotational splitting and tunneling motion

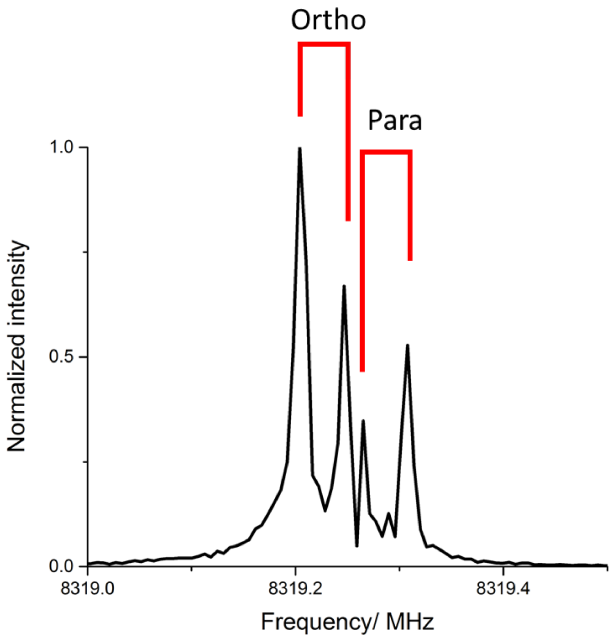

Figure 3. 3 The splitting due to the water tunneling motion of the 110-000 transition.

1) Water tunneling motion

The tunneling splittings observed in the spectra are ascribed to the interchange of the bonded and nonbonded hydrogen atoms of the H_2O subunit in the complex (Figure 3.3). Similar splittings were reported for the TFE···water system, although not in the ethanol···water and methyl lactate···water systems. In the ethanol···water case, the study was carried out using a chirped pulse FTMW instrument with lower resolution. The appearance of water tunneling motion is strongly dependent on the strength of the intermolecular hydrogen bond between Hw

and proton acceptor function group. Comparing to the F atom as the hydrogen bond acceptor in both 2-FE and TFE cases, O atoms in either carbonyl group (as in methyl lactate···water dimer) or hydroxyl group (presented in the ethanol···water complex) exhibit a greater hydrogen

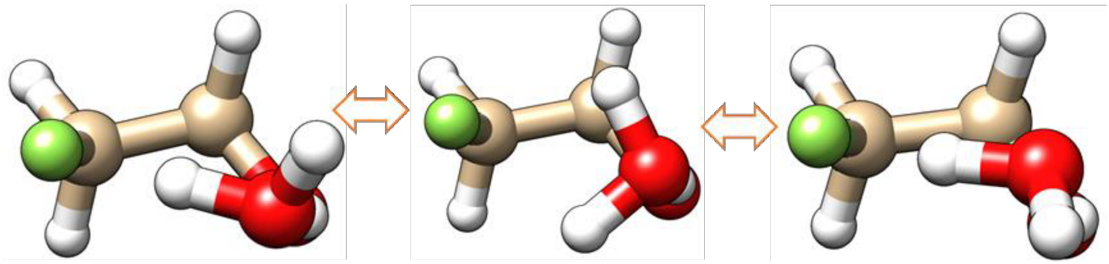

Figure 3. 4 The tunneling motion of the water molecule: interchange between H-bonded and non-H-bonded H atoms of water

bonding strength and thus reduce the probability of water tunneling. The directionality of hydrogen bonding may also attribute to its stability, since in fluorinated alcohol water complexes the hydrogen bond angles are around 140-150°, much away from linearity.

As stated before, the water tunneling motion is the interchange between bonded hydrogen atom and unbounded hydrogen. This interchange happens because the O-H···O hydrogen bond can rotate along the oxygen atom's lone pair. The rotation about the oxygen atom of water is presented in the diagram (Figure 3.4). The tunneling barrier is estimated theoretically to be 7.0 kJ/mol.

2) Hydrogen wagging motion

In order to justify the true experimental geometry of the dimer, the wagging motion (Figure 3.5) of the unbonded hydrogen atom in the water molecule is one critical determinant. This motion, as discussed in theoretical calculation part before, is the interchange of the two lone pairs in the oxygen atom in water molecule. This motion is in fact a vibrational motion, and has a comparably large amplitude which could alter the dipole moment drastically.

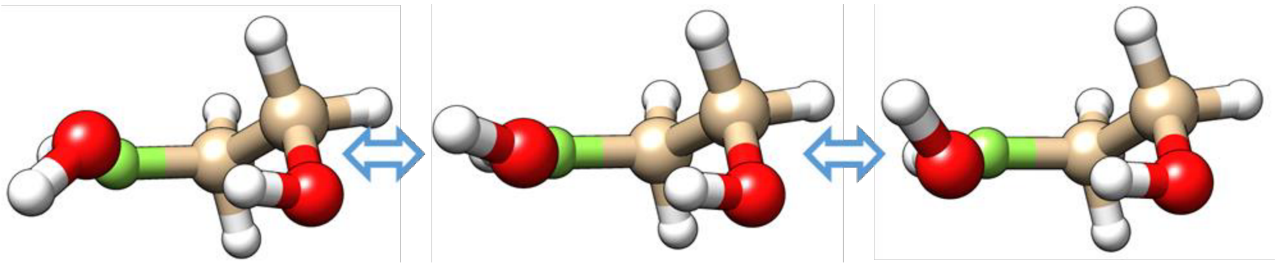

Figure 3. 5 The hydrogen tunneling motion of water molecule: wagging motion of the unbonded hydrogen atom

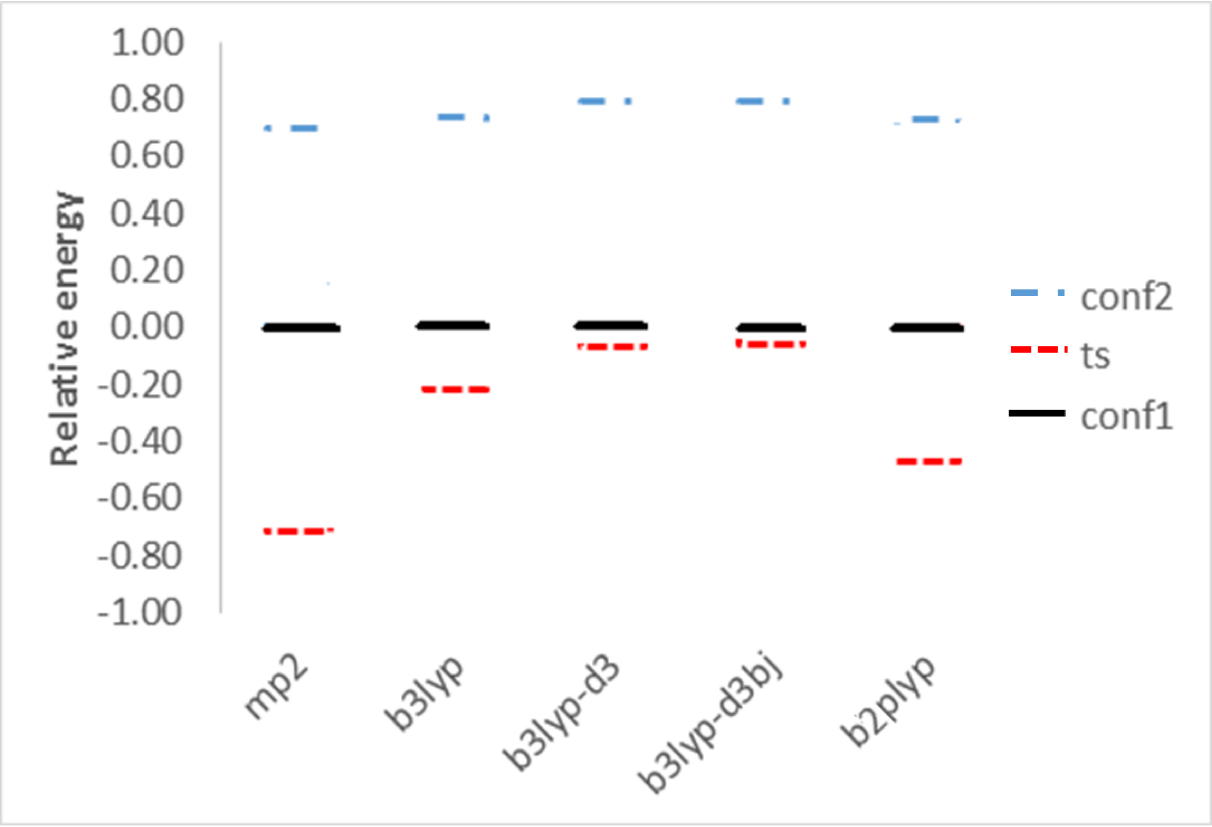

Figure 3. 6 The energy calculation results for conf I, conf II and transition state. The energy are presented as relative energy while all zero points are the energy of conformer I under different theories.

Transitions state calculations have been done for this motion in different types of theories (same 6-311++G(2d,p) basis set) (Figure 3.6). The calculated results are presented in the following graphs. It is clear that no matter which theories we use, the conformer 1 is always more stable than conformer 2, and the relative energy difference is similar between theories (about 0.7 kJ/mol). As for transition states, it is interesting to see that after zero-point energy correction transition state is predicted to have lower energy than conformer 1 in all theories. The low-lying transition state indicates that the transition between conformer 1 and conformer 2 is essentially barrier less. In other words, there should be no two different minima but just one global minimum sitting somewhere in between these two. If we look at the transition state

calculation under different theories, we found that although it is always below conformer 1 in energy, the difference differs a lot between theories. The mp2 and b3lyp/b2plyp theories predicted a bigger energy gap while b3lyp-d3 and b3lyp-d3bj provided a closer difference in energy. One possible explanation is that the last two theories incorporate the dispersion correction into the calculation. The dispersion correction captures the large amplitude motion of the hydrogen atom better and therefore brings the transition state energy higher.

Potential energy scan has also been done in mp2/6-311++G(2d,p) level to further understand this motion (Figure 3.7). The scan of the dihedral angle F7-H11-O10-H12 reproduces the wagging motion and as one can see from the scan curve, also reproduces the two minima conf 1 and conf 2. The barrier in the scan is about 0.5 kJ/mol before ZPE correction. And after ZPE correction only one uniform zero-point can be 'feel' by the molecule. That being said, the overall wave function would be similar to one anharmonic potential wave function, with slightly tile towards the lower energy conformer 1. The experimental geometry then, would be the averaged structure between two optimized minima. Such large amplitude motion can help to interpret some unique experimental observations such as the magnitude of the c-dipole moment

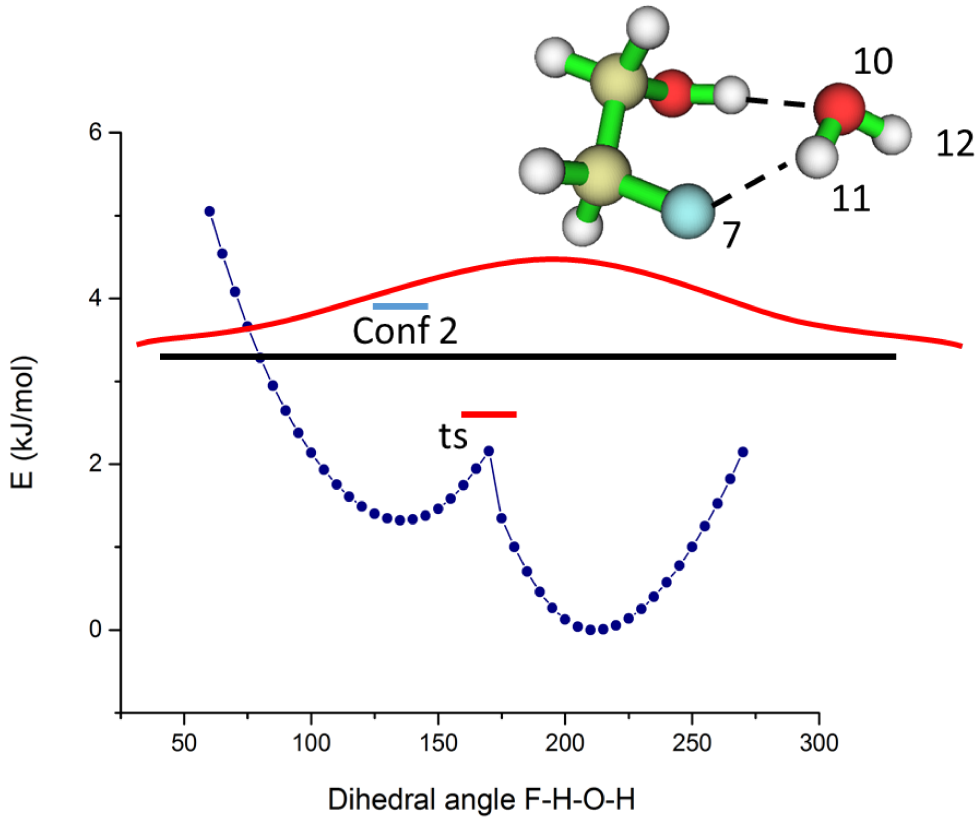

Figure 3. 7 The potential energy scan for the dihedral angle F7-H11-O10-H12. The energies shown are relative energies with respect to the lowest energy position. The black line is the ground state with ZPE correction, the red line indicates the TS and the blue line is for conf II, with ZPE corrections.

component and the position of the free hydrogen atom in water. It also appears that the MP2 energy ordering for I and II is just the opposite of the experimentally observed trend.

3.4.3 Deuterium substitution study

Isotopic studies of the system have also been done in order to gain futher insight into the conformation of the 2-FE···water dimer. All possible deuterium isotopologues of the 2-FE···water dimer have been studied, 2-FE···D_2O, 2-FE···DOH, 2-FE···HOD, 2-FEOD···D_2O, 2-FEOD···DOH, 2-FEOD···HOD (2-FEOD is the deuterium substituted 2-FE at the hydroxyl hydrogen) and 2-FEOD···H_2O. A similar spectral fitting procedure was used for all the isotopologues and the resulting spectroscopic constants are listed in Table 3.4, 3.5. 2-FE···DOH refers to the situation where the bonded H atom of the water subunit is replaced by a D atom, while 2-FE···HOD refers to the case where the nonbonded H atom of water is replaced by a D atom. After the deuterium substitution, two original equivalent H atoms of water in 2-FE···H_2O are no longer equivalent, or in other words, 2-FE···HOD and 2-FE···DOH are not degenerate geometries (Figure 3.8). In fact, we observed each with a distinct set of rotational constants, corresponding to their specific mass distributions. For the cases of 2-FE···D_2O and 2-FEOD···D_2O isotopologues, although the two D atoms are still equivalent, D is much heavier and the tunnelling splittings are expected to be much smaller than those of Hs. Small splittings of a few to tens of kHz have also been observed for all these D-isotopologues, we ascribed them to the nuclear quadrupole splitting of deuterium atom and used the estimated center frequencies for

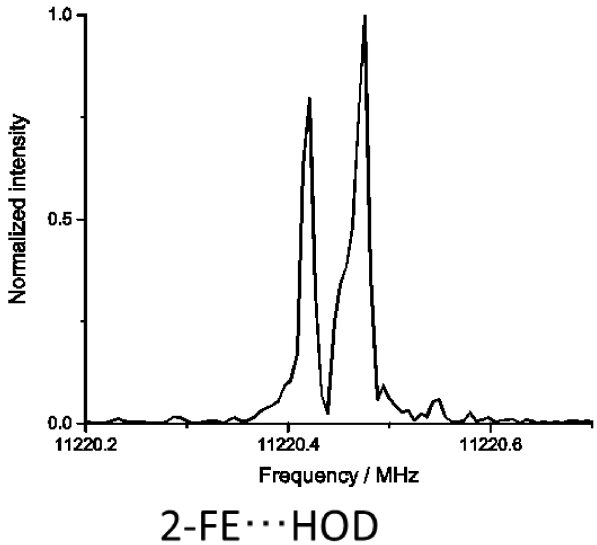

Figure 3. 8 The water tunneling splitting is quenched when one of the hydrogen atom is substituted by deuterium atom.

the final spectroscopic fits. For 2-FEOD···H_2O, one also expects similar tunneling splittings as

in 2-FE···H_2O. However, such tunneling splittings were obscured by the nuclear quadrupole splitting of deuterium atom and no detailed analysis was carried out (Table 3.6, 3.7).

Table 3. 4 Experimental spectroscopic constants obtained for four deuterium substituted 2-fluroethaonol monohydrates

Parameter	2-FE···DOH	2-FE···HOD	2-FE···D_2O	2-FEOD···DOH
A (MHz)	4911.8767(21)	4945.7938(20)	4906.2832(24)	4844.0356(25)
B (MHz)	3314.3815(33)	3173.2735(40)	3129.3620(47)	3305.0418(49)
C (MHz)	2143.4969(22)	2091.5787(18)	2066.4340(21)	2127.2467(20)
D_J (kHz)	3.56(14)	4.31(21)	2.88(24)	4.38(26)
D_K (kHz)	2.22	2.22	2.22	2.22
D_{JK} (kHz)	1.68	1.68	1.68	1.68
d_J (kHz)	-1.17(13)	-1.65(18)	1.05(21)	-1.35(22)
d_K (kHz)	-0.54	-0.54	-0.54	-0.54
N	15	14	14	14
σ (kHz)	5.9	4.6	5.5	5.3

Table 3. 5 Experimental spectroscopic constants obtained for other three deuterium substituted 2-fluroethaonol monohydrates

Parameter	2-FEOD···HOD	2-FEOD···H_2O	2-FEOD···D_2O
A (MHz)	4880.1838(29)	4889.0540(25)	4838.0906(23)
B (MHz)	3164.7939(61)	3354.2133(50)	3122.4642(45)
C (MHz)	2076.6828(20)	2155.1995(20)	2051.8292(20)
D_J (kHz)	3.33(31)	6.15(27)	3.02(24)
D_K (kHz)	2.22	2.22	2.22
D_{JK} (kHz)	1.68	1.68	1.68

d_J (kHz)	-0.93(27)	2.54(23)	-0.82(21)
d_K (kHz)	-0.54	-0.54	-0.54
N	13	14	14
σ (kHz)	4.7	5.4	5.2

Table 3. 6 Measured rotational transition frequencies of four deuterium substituted monohydrated.

	2FE···DOH		2FE···HOD		2FE···D_2O		2FEOD···DOH	
J'Ka'Kc'-J"Ka"Kc"	ν_{exp}/kHz	Δν/kHz	ν_{exp}/kHz	Δν/kHz	ν_{exp}/kHz	Δν/kHz	ν_{exp}/kHz	Δν/kHz
111-000	7055.3598	1.4	7037.3551	-1.1	6972.7026	-0.6	6971.2649	0.3
221-212	8226.2280	-5.7	8119.0322	-5.6	8035.6160	-8.9	8149.0485	-0.4
110-000	8305.0481	1.4	8562.5364	1.4	8519.4537	4.3	8150.2602	-7.4
202-111	8870.1313	6.4	8392.1257	2.9	8261.0474	-0.9	8861.7857	-1.3
212-111	9744.7883	-0.5	9447.9188	1.1	9328.5932	-3.0	9686.6741	-4.0
322-313	10303.5597	1.7						
202-101	10467.6143	-4.9	10164.6452	1.1	10037.9691	2.0	10400.7794	-1.3
212-101	11342.2836	0.5	11220.4412	2.2	11105.5254	10.4	11225.6645	-7.3
211-110	12086.4905	7.2	11611.1944	-7.3	11454.3908	1.4	12042.1889	6.9
303-212	14017.7270	-14.0	13488.5233	-7.6	13304.3175	-4.2	13952.5235	-5.2
313-212	14374.7554	4.8	13971.8533	1.9	13798.8935	6.1	14279.8308	3.4
211-101	14854.8522	-0.7	14465.4135	9.0	14294.2352	5.3	14758.9599	-0.1
303-202	14892.4019	-3.0	14544.3320	6.2	14371.8628	-6.8	14777.4126	-7.2
313-202	15249.4258	11.3	15027.6445	-1.8	14866.4382	3.0	15104.7274	8.9
221-110	16878.9558	-4.5	16928.7675	-3.6	16785.1163	-7.6	16659.1686	7.2

Table 3. 7 Measured rotational transition frequencies of four deuterium substituted monohydrated.

	2FEOD···HOD		2FEOD···H_2O		2FEOD···D_2O	
J'Ka'Kc'-J"Ka"Kc"	ν_{exp}/kHz	Δν/kHz	ν_{exp}/kHz	Δν/kHz	ν_{exp}/kHz	Δν/kHz
111-000	6956.8538	2.5	7044.2245	-7.9	6889.9123	6.9
221-212	8410.4200	1.0	8243.2325	4.4	7960.5269	-7.0
110-000			8201.4031	-8.6	8358.6991	-5.1
202-111	8390.2066	0.6	9005.4451	-5.1	8265.9040	-2.0
212-111	9394.7509	-7.5	9819.6941	6.8	9277.8685	-6.0
202-101	10105.5903	-3.7	10540.2880	-6.4	9981.5278	-2.3
212-101	11110.1575	11.1	11354.5258	-5.8	10993.4984	-0.2
211-110	11570.9226	1.3	12217.5591	2.4	11419.0947	2.5
303-212	13436.7484	4.1	14153.0429	-4.4	13258.9776	-4.7
313-212	13885.9246	-2.4	14471.7669	0.0	13716.0138	8.1
211-101	14374.4147	1.7	14951.3988	2.3	14205.3516	6.8
303-202	14441.2924	-4.2	14967.2863	1.9	14270.9436	-7.2
313-202	14890.4824	3.0	15286.0060	1.9	14727.9781	3.9
221-110	16717.0682	-5.4	16822.1120	8.6	16565.9513	1.2

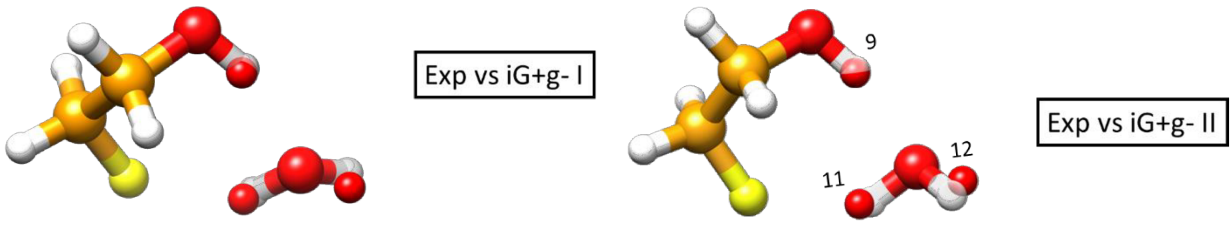

Figure 3. 9 Kraitchman coordinate substitution structures of the 2-FE···H_2O comparing with iG+g- I and iG+g- II.

The Kraitchman structures[21] were calculated from the rotational constants of isotopologues and shown in Figure 3.9. The position of hydrogen atom in hydroxyl group of 2-FE was calculated by isotopic data of 2-FEOD···H_2O. The hydrogen atom coordinates in water were calculated through the substitution of respective deuterated isotopologues in2-FE···H_2O (Table 3.8). The resulting structure from experimental spectroscopic constants shows a better agreement with the iG+g- II 2-FE···H_2O geometry for the position of the hydroxyl hydrogen atom in 2-FE and for that of the bonded hydrogen atom in water. The above experimental analysis in return supports the conclusion that the observed conformer is more an averaging structure between the iG+g- I and iG+g- II.

Table 3. 8 Substitution coordinates of the monohydrate and the theoretical coordinates

	Exp	iG+g- I	iG+g- II		Exp	iG+g- I	iG+g- II		Exp	iG+g- I	iG+g- II
D9				D11				D12			
a	±0.823	0.835	0.810	a	±1.496	1.637	1.673	a	±2.997	3.001	2.865
b	±1.100	1.129	1.129	b	±0.922	-0.906	-0.888	b	±0.000	-0.291	-0.193
c	±0.213	-0.292	-0.220	c	±0.248	0.009	0.073	c	±0.429	-0.351	0.760

3.5 Theoretical calculation of 2-FE···$(H_2O)_2$

Theoretical calculation for the dihydrate complexes of 2-fluoroethanol has also been done (Table 3.9). The possible orientation of the second water can be inserted into the intermolecular

hydrogen bond of monohydrates, adducted to the oxygen atom lone pairs or adducted to the fluorine atom lone pairs. The 2-FE conformation can also have 5 different possibilities. After careful conformation search and optimization, 12 local minima are identified and here presents the most stable four trimers after zero-point energy corrections (Figure 3.10).

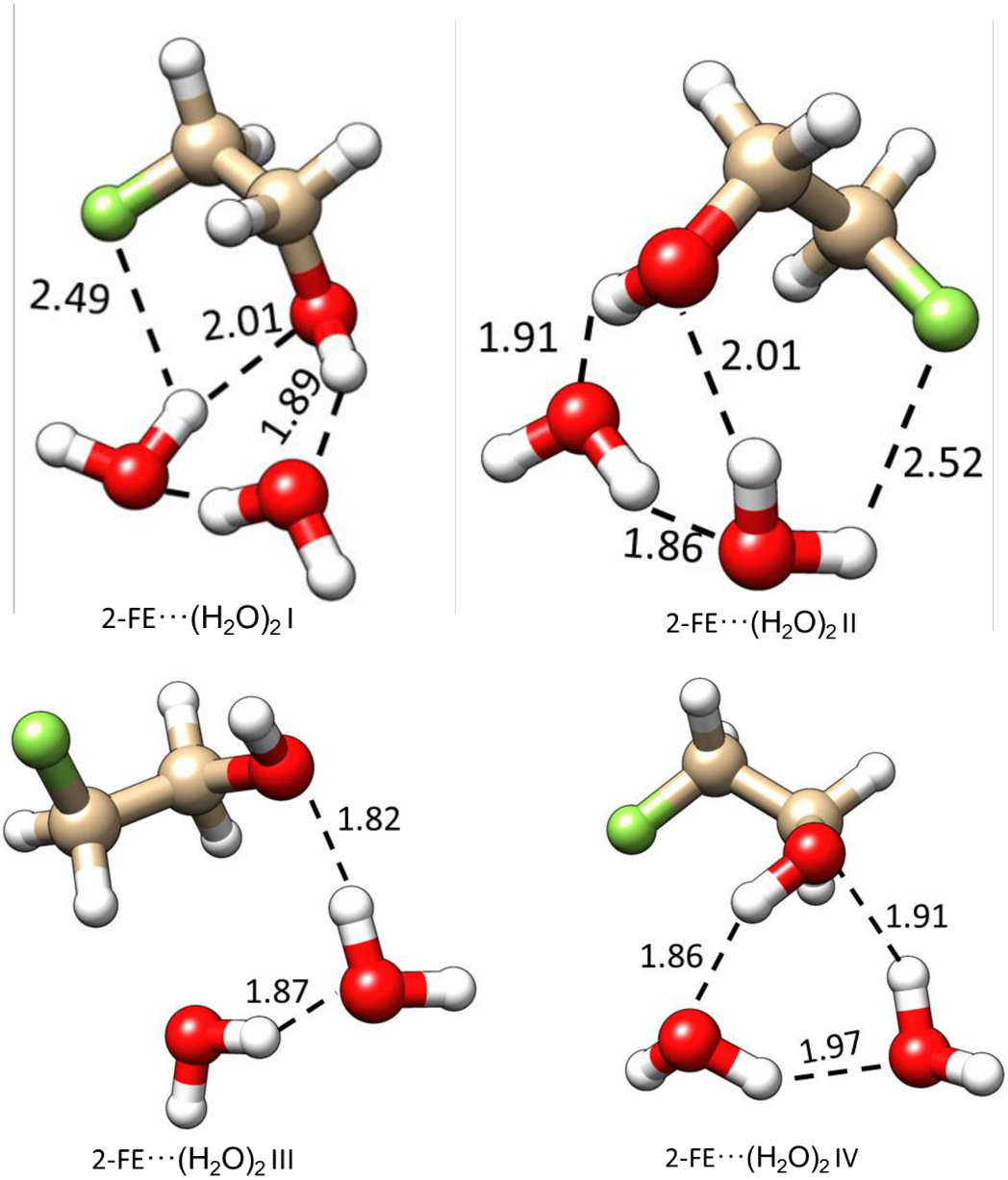

Figure 3. 10 Optimized geometries of 2-FE···$(H_2O)_2$ conformers. Intermolecular hydrogen bonds are indicated with dash lines. (MP2/6-311++G(2d,p)

Table 3. 9 Raw energies and relative energies of dehydrate conformers.

	2-FE···$(H_2O)_2$ I	2-FE···$(H_2O)_2$ II	2-FE···$(H_2O)_2$ III	2-FE···$(H_2O)_2$ IV
ΔD_e (kJ/mol)	0	0.42	-4.93	-3.83
ΔD_0 (kJ/mol)	0	-0.77	-3.71	-3.77

From the calculation results one can easily recognize that the formation of the 2-FE in the two most stable conformers are not the same. The conformer 2-FE···$(H_2O)_2$ II has the lowest raw energy, while after zero-point energy correction, the 2-FE···$(H_2O)_2$ I becomes the most stable trimer. The 2-fluoroethanol conformation in 2-FE···$(H_2O)_2$ I is G+g-, which is consistent with the lowest energy monomer or monohydrate. The second water molecule in this dehydrate conformer, in fact, inserts into the intermolecular hydrogen bond between F atom in 2-FE and H atom from water molecule. The 2-FE···$(H_2O)_2$ II conformer, however, takes the G+g+ conformation for 2-FE which has a much higher energy comparing to G+g-. The energy difference between the two lowest energy trimers is only 0.8 kJ/mol after correction, indicating the insertion of extra water molecule will have some impact on the conformation of fluoroethanol and we would expect to see both conformers with fair intensities in supersonic jet expansion.

3.6 Summary

In summary, the pure rotational spectrum of 2-fluoroethanol monohydrate complex has been studied using chirped-pulse and cavity-based FTMW spectroscopy. Tunneling splittings were observed and confirmed to be the result of interchange between bonded and unbonded hydrogen atoms in water molecule. Both tunneling components were unambiguously assigned. Seven deuterium substituted isotopologues of 2-fluoroethanol and water dimers have been detected and assigned. Based on the structural fit from isotopic substitution, the conformation of the complex is in between of two insertion conformers that are connected by oxygen wagging motion. The tunneling dynamic of the wagging motion has been theoretically studied. The

vibration of the oxygen atom in water molecule is essentially barrierless, leading to an average geometry and a non-zero c-type dipole moment.

---

1. M. BUCK, *Quarterly Reviews of Biophysics*, 1998, **31**, 297-355.
2. A. Jasanoff and A. R. Fersht, *Biochemistry*, 1994, **33**, 2129-2135.
3. D.-P. Hong, M. Hoshino, R. Kuboi and Y. Goto, *J. Am. Chem. Soc.*, 1999, **121**, 8427-8433.
4. J. F. Povey, C. M. Smales, S. J. Hassard and M. J. Howard, *Journal of Structural Biology*, 2007, **157**, 329-338.
5. D. Roccatano, G. Colombo, M. Fioroni and A. E. Mark, *Proceedings of the National Academy of Sciences of the United States of America*, 2002, **99**, 12179-12184.
6. H. C. Hoffmann, S. Paasch, P. Muller, I. Senkovska, M. Padmanaban, F. Glorius, S. Kaskel and E. Brunner, *Chem Commun (Camb)*, 2012, **48**, 10484-10486.
7. K. S. Buckton and R. G. Azrak, *Journal of Chemical Physics*, 1970, **52**, 5652-5655.
8. X. C. Liu, N. Borho and Y. J. Xu, *Chemistry-a European Journal*, 2009, **15**, 270-277.
9. J. Thomas and Y. J. Xu, *Journal of Chemical Physics*, 2014, **140**, 5.
10. I. A. Finneran, P. B. Carroll, M. A. Allodi and G. A. Blake, *Physical Chemistry Chemical Physics*, 2015, **17**, 24210-24214.
11. M. Heger, T. Scharge and M. A. Suhm, *Physical Chemistry Chemical Physics*, 2013, **15**, 16065-16073.
12. J. Thomas and Y. J. Xu, *Journal of Physical Chemistry Letters*, 2014, **5**, 1850-1855.
13. J. Thomas, X. C. Liu, W. Jager and Y. J. Xu, *Angew. Chem.-Int. Edit.*, 2015, **54**, 11711-11715.
14. J. Thomas, O. Sukhorukov, W. Jager and Y. J. Xu, *Angew. Chem.-Int. Edit.*, 2013, **52**, 4402-4405.
15. S. Ghosh, J. Thomas, W. Huang, Y. Xu and W. Jäger, *The Journal of Physical Chemistry Letters*, 2015, **6**, 3126-3131.
16. M. J. Frisch, G. W. Trucks, H. B. Schlegel, G. E. Scuseria, M. A. Robb, J. R. Cheeseman, G. Scalmani, V. Barone, B. Mennucci, G. A. Petersson, H. Nakatsuji, M. Caricato, X. Li, H. P. Hratchian, A. F. Izmaylov, J. Bloino, G. Zheng, J. L. Sonnenberg, M. Hada, M. Ehara, K. Toyota, R. Fukuda, J. Hasegawa, M. Ishida, T. Nakajima, Y. Honda, O. Kitao, H. Nakai, T. Vreven, J. A. Montgomery Jr., J. E. Peralta, F. Ogliaro, M. J. Bearpark, J. Heyd, E. N. Brothers, K. N. Kudin, V. N. Staroverov, R. Kobayashi, J. Normand, K. Raghavachari, A. P. Rendell, J. C. Burant, S. S. Iyengar, J. Tomasi, M. Cossi, N. Rega, N. J. Millam, M. Klene, J. E. Knox, J. B. Cross, V. Bakken, C. Adamo, J. Jaramillo, R. Gomperts, R. E. Stratmann, O. Yazyev, A. J. Austin, R. Cammi, C. Pomelli, J. W. Ochterski, R. L. Martin, K. Morokuma, V. G. Zakrzewski, G. A. Voth, P. Salvador, J. J. Dannenberg, S. Dapprich, A. D. Daniels, Ö. Farkas, J. B. Foresman, J. V. Ortiz, J. Cioslowski and D. J. Fox, *Journal*, 2009.
17. S. F. Boys and F. Bernardi, *Molecular Physics*, 1970, **19**, 553-566.
18. C. M. Western, *University of Bristol: Bristol, U. K.* http://Pgopher.chm.bris.ac.uk.
19. J. Thomas, O. Sukhorukov, W. Jager and Y. Xu, *Angewandte Chemie*, 2014, **53**, 1156-1159.

20. C. Merten and Y. Xu, *Angewandte Chemie*, 2013, **52**, 2073-2076.
21. J. Kraitchman, *Am J Phys*, 1953, **21**, 17-24.

Chapter 4

Concluding remarks

The fluoroethanol and water cosolvent can alter the secondary and tertiary structures of proteins and polypeptides. Although the mechanism behind the above phenomenon is still far from understood, it is commonly believed that intermolecular hydrogen bonding plays an important role. It is clear that to understand such mechanism in detail, multiple approaches are necessary. Using the bottom-up approach, we examine the hydrogen bonding details in small hydrated fluoroethanol molecular clusters. In particular, in the current thesis, microwave spectroscopic techniques have been employed to explore the structure and tunneling dynamic of the 2-fluoroethanol (2-FE)···water complex, complemented with high level theoretical computation. Both cavity-based and chirped-pules Fourier transform microwave sectrometers have been used to carry out the experimental study.

Pure rotational spectra of the 2-FE···H_2O dimer, as well as its seven isotopologues have been detected and analyzed. The preferred binding topology is established to be an insertion topology, where the water is inserted into the existing OH···FC contact ring. Some narrow splittings have been detected in each rotational transition of 2-FE···H_2O. Based on the relative intensity and subsequent isotopic study, such splittings are unambiguously ascribed as due to the tunneling motion which exchanges the bonded and nonbonded H atoms in the water subunit in the complex. Another motion is the wagging motion of the non-bonded hydrogen atom in the water subunit from above and below the heavy atom H-bonded ring plane, which connects two local minimum geometries. This motion is best described as a large amplitude wagging motion since the motion is barrierless. This gives rise to a complicated averaging between the two inequivalent minima, i.e. iG+g- I and iG+g- II.

Through this thesis study, the hydrogen bonding typologies, water tunneling dynamics and large amplitude motion of 2-FE···H_2O have been examined in detail, providing us with more insight about the interactions between 2-fluoroalcohols and water.

It would be desirable to study larger hydrated clusters with more water molecules in order to build a better understanding about the water and 2-fluoroethanol co-solvent. Dihydrate and even larger hydrate complexes have already been studied using both cavity and chirped pulse Fourier transform microwave spectroscopy in conjunction with a supersonic jet expansion. For example, the dihydrate of acetic acid has been studied using a cavity-based microwave spectrometer.[1] The experimental observation confirmed the extensive hydrogen bonded ring

structure predicted by theoretical calculations, in which the second water molecule is inserted into the preexisting hydrogen bonded ring. Similar H-bonded topology was also reported for the trihydrate complex of nitric acid.[2] Therefore, it is interesting to find out the position of second or third water molecules and analyze the possible tunneling and/or large amplitude motions of the water subunits in these larger hydrates. This stepwise solvation approach will allow one to gain insight into the first few steps of co-solvation in the 2-fluroroethanol and water mixture.

---

1. B. Ouyang and B. J. Howard, *Physical Chemistry Chemical Physics*, 2009, **11**, 366-373.
2. G. Sedo, J. L. Doran and K. R. Leopold, *Journal of Physical Chemistry A*, 2009, **113**, 11301-11310.

Bibliography

1. A. D. McNaught, A. Wilkinson, M. Nic, J. Jirat and B. Kosata, *IUPAC. Compendium of Chemical Terminology, 2nd ed. (the "Gold Book")*, Blackwell Scientific Publications, Oxford, 1997.
2. E. Arunan, G. R. Desiraju, R. A. Klein, J. Sadlej, S. Scheiner, I. Alkorta, D. C. Clary, R. H. Crabtree, J. J. Dannenberg and P. Hobza, *Pure and applied chemistry*, 2011, **83**, 1637-1641.
3. P. A. Kollman and L. C. Allen, *Chemical Reviews*, 1972, **72**, 283-303.
4. G. A. Jeffrey, *An Introduction to Hydrogen Bonding*, Oxford University Press, 1997.
5. T. Steiner, *Angewandte Chemie International Edition*, 2002, **41**, 48-76.
6. L. Pauling, *The Nature of the Chemical Bond and the Structure of Molecules and Crystals: An Introduction to Modern Structural Chemistry*, Cornell University Press, 1960.
7. T. S. Moore and T. F. Winmill, *Journal of the Chemical Society*, 1912, **101**, 1635-1676.
8. W. M. Latimer and W. H. Rodebush, *J. Am. Chem. Soc.*, 1920, **42**, 1419-1433.
9. A. S. N. Murthy and C. N. R. Rao, *Applied Spectroscopy Reviews*, 1968, **2**, 69-191.
10. K. Biradha and M. J. Zaworotko, *J. Am. Chem. Soc.*, 1998, **120**, 6431-6432.
11. L. S. Birchall, S. Roy, V. Jayawarna, M. Hughes, E. Irvine, G. T. Okorogheye, N. Saudi, E. De Santis, T. Tuttle and A. A. Edwards, *Chemical Science*, 2011, **2**, 1349-1355.
12. P. Ottiger, C. Pfaffen, R. Leist, S. Leutwyler, R. A. Bachorz and W. Klopper, *The Journal of Physical Chemistry B*, 2009, **113**, 2937-2943.
13. S. J. Grabowski and P. Lipkowski, *The Journal of Physical Chemistry A*, 2011, **115**, 4765-4773.
14. N. V. Belkova, E. S. Shubina and L. M. Epstein, *Accounts Chem Res*, 2005, **38**, 624-631.
15. E. S. Shubina, N. V. Belkova and L. M. Epstein, *Journal of Organometallic Chemistry*, 1997, **536**, 17-29.
16. L. M. Epstein, E. S. Shubina, A. N. Krylov, A. Z. Kreindlin and M. I. Rybinskaya, *Journal of Organometallic Chemistry*, 1993, **447**, 277-280.
17. Y. Marechal, *The Hydrogen Bond and the Water Molecule: The Physics and Chemistry of Water, Aqueous and Bio-Media*, Elsevier Science, 2006.
18. S. SenGupta, H. P. Upadhyaya, A. Kumar and P. D. Naik, *Chem Phys*, 2014, **443**, 8-16.
19. O. Dopfer, G. Lembach, T. G. Wright and K. Mullerdethlefs, *Journal of Chemical Physics*, 1993, **98**, 1933-1943.
20. M. Broquier, F. Lahmani, A. Zehnacker-Rentien, V. Brenner, P. Millie and A. Peremans, *Journal of Physical Chemistry A*, 2001, **105**, 6841-6850.
21. G. G. Yee, J. L. Fulton and R. D. Smith, *Journal of Physical Chemistry*, 1992, **96**, 6172-6181.
22. R. H. Wu and T. B. McMahon, *ChemPhysChem*, 2008, **9**, 2826-2835.
23. T. Goldstein, M. S. Snow and B. J. Howard, *Journal of Molecular Spectroscopy*, 2006, **236**, 1-10.

24. S. Melandri, A. Maris, P. G. Favero and W. Caminati, *ChemPhysChem*, 2001, **2**, 172-177.
25. S. Melandri, B. M. Giuliano, A. Maris, L. B. Favero, P. Ottaviani, B. Velino and W. Caminati, *Journal of Physical Chemistry A*, 2007, **111**, 9076-9079.
26. C. Perez, D. P. Zaleski, N. A. Seifert, B. Temelso, G. C. Shields, Z. Kisiel and B. H. Pate, *Angew. Chem.-Int. Edit.*, 2014, **53**, 14368-14372.
27. G. Feng, L. B. Favero, A. Maris, A. Vigorito, W. Caminati and R. Meyer, *J. Am. Chem. Soc.*, 2012, **134**, 19281-19286.
28. J. Thomas and Y. J. Xu, *Journal of Physical Chemistry Letters*, 2014, **5**, 1850-1855.
29. I. A. Finneran, P. B. Carroll, M. A. Allodi and G. A. Blake, *Physical Chemistry Chemical Physics*, 2015, **17**, 24210-24214.
30. C. Merten and Y. Xu, *Angewandte Chemie*, 2013, **52**, 2073-2076.
31. G. Feng, Q. Gou, L. Evangelisti and W. Caminati, *Angew. Chem.-Int. Edit.*, 2014, **53**, 530-534.
32. K. Brendel, H. Mäder, Y. Xu and W. Jäger, *Journal of Molecular Spectroscopy*, 2011, **268**, 47-52.
33. R. G. Parr, D. P. Craig and I. G. Ross, *The Journal of chemical physics*, 1950, **18**, 1561-1563.
34. L. C. Allen and A. M. Karo, *Reviews of Modern Physics*, 1960, **32**, 275-285.
35. S. Scheiner, *Hydrogen Bonding: A Theoretical Perspective*, Oxford University Press, 1997.
36. J. Thomas, X. C. Liu, W. Jager and Y. J. Xu, *Angew. Chem.-Int. Edit.*, 2015, **54**, 11711-11715.
37. S. F. Boys and F. Bernardi, *Molecular Physics*, 1970, **19**, 553-566.
38. S. Melandri, D. Consalvo, W. Caminati and P. G. Favero, *Journal of Chemical Physics*, 1999, **111**, 3874-3879.
39. S. P. Dempster, O. Sukhorukov, Q.-Y. Lei and W. Jäger, *The Journal of chemical physics*, 2012, **137**, 174303.
40. F. X. Sunahori, N. Borho, X. Liu and Y. Xu, *The Journal of chemical physics*, 2011, **135**, 234310.
41. K. B. M. Jr., R. H. Hughes and E. B. W. Jr., *Review of Scientific Instruments*, 1949, **20**, 821-826.
42. R. H. Hughes and E. B. Wilson Jr, *Physical Review*, 1947, **71**, 562.
43. T. J. Balle, *Review of Scientific Instruments*, 1981, **52**, 33.
44. S. Ghosh and W. Jäger, master of science Thesis, University of Alberta, 2015.
45. S. Fölling, S. Trotzky, P. Cheinet, M. Feld, R. Saers, A. Widera, T. Müller and I. Bloch, *Nature*, 2007, **448**, 1029-1032.
46. Y. Xu and W. Jäger, *The Journal of chemical physics*, 1997, **106**, 7968-7980.
47. G. G. Brown, B. C. Dian, K. O. Douglass, S. M. Geyer, S. T. Shipman and B. H. Pate, *Review of Scientific Instruments*, 2008, **79**, 053103.
48. J. Thomas, J. Yiu, J. Rebling, W. Jager and Y. Xu, *The journal of physical chemistry. A*, 2013, **117**, 13249-13254.
49. C. M. Western, *University of Bristol: Bristol, U. K.* http://Pgopher.chm.bris.ac.uk.
50. N. A. Seifert, I. A. Finneran, C. Perez, D. P. Zaleski, J. L. Neill, A. L. Steber, R. D. Suenram, A. Lesarri, S. T. Shipman and B. H. Pate, *Journal of Molecular Spectroscopy*, 2015, **312**, 13-21.

51. M. BUCK, *Quarterly Reviews of Biophysics*, 1998, **31**, 297-355.
52. A. Jasanoff and A. R. Fersht, *Biochemistry*, 1994, **33**, 2129-2135.
53. D.-P. Hong, M. Hoshino, R. Kuboi and Y. Goto, *J. Am. Chem. Soc.*, 1999, **121**, 8427-8433.
54. J. F. Povey, C. M. Smales, S. J. Hassard and M. J. Howard, *Journal of Structural Biology*, 2007, **157**, 329-338.
55. D. Roccatano, G. Colombo, M. Fioroni and A. E. Mark, *Proceedings of the National Academy of Sciences of the United States of America*, 2002, **99**, 12179-12184.
56. H. C. Hoffmann, S. Paasch, P. Muller, I. Senkovska, M. Padmanaban, F. Glorius, S. Kaskel and E. Brunner, *Chem Commun (Camb)*, 2012, **48**, 10484-10486.
57. K. S. Buckton and R. G. Azrak, *Journal of Chemical Physics*, 1970, **52**, 5652-5655.
58. X. C. Liu, N. Borho and Y. J. Xu, *Chemistry-a European Journal*, 2009, **15**, 270-277.
59. J. Thomas and Y. J. Xu, *Journal of Chemical Physics*, 2014, **140**, 5.
60. M. Heger, T. Scharge and M. A. Suhm, *Physical Chemistry Chemical Physics*, 2013, **15**, 16065-16073.
61. J. Thomas, O. Sukhorukov, W. Jager and Y. J. Xu, *Angew. Chem.-Int. Edit.*, 2013, **52**, 4402-4405.
62. S. Ghosh, J. Thomas, W. Huang, Y. Xu and W. Jäger, *The Journal of Physical Chemistry Letters*, 2015, **6**, 3126-3131.
63. M. J. Frisch, G. W. Trucks, H. B. Schlegel, G. E. Scuseria, M. A. Robb, J. R. Cheeseman, G. Scalmani, V. Barone, B. Mennucci, G. A. Petersson, H. Nakatsuji, M. Caricato, X. Li, H. P. Hratchian, A. F. Izmaylov, J. Bloino, G. Zheng, J. L. Sonnenberg, M. Hada, M. Ehara, K. Toyota, R. Fukuda, J. Hasegawa, M. Ishida, T. Nakajima, Y. Honda, O. Kitao, H. Nakai, T. Vreven, J. A. Montgomery Jr., J. E. Peralta, F. Ogliaro, M. J. Bearpark, J. Heyd, E. N. Brothers, K. N. Kudin, V. N. Staroverov, R. Kobayashi, J. Normand, K. Raghavachari, A. P. Rendell, J. C. Burant, S. S. Iyengar, J. Tomasi, M. Cossi, N. Rega, N. J. Millam, M. Klene, J. E. Knox, J. B. Cross, V. Bakken, C. Adamo, J. Jaramillo, R. Gomperts, R. E. Stratmann, O. Yazyev, A. J. Austin, R. Cammi, C. Pomelli, J. W. Ochterski, R. L. Martin, K. Morokuma, V. G. Zakrzewski, G. A. Voth, P. Salvador, J. J. Dannenberg, S. Dapprich, A. D. Daniels, Ö. Farkas, J. B. Foresman, J. V. Ortiz, J. Cioslowski and D. J. Fox, *Journal*, 2009.
64. J. Thomas, O. Sukhorukov, W. Jager and Y. Xu, *Angewandte Chemie*, 2014, **53**, 1156-1159.
65. J. Kraitchman, *Am J Phys*, 1953, **21**, 17-24.
66. B. Ouyang and B. J. Howard, *Physical Chemistry Chemical Physics*, 2009, **11**, 366-373.
67. G. Sedo, J. L. Doran and K. R. Leopold, *Journal of Physical Chemistry A*, 2009, **113**, 11301-11310.